Dynamics and fragmentation of van der Waals clusters: $(H_2O)_n$, $(CH_3OH)_n$, and $(NH_3)_n$ upon ionization by a 26.5 eV soft x-ray laser

F. Dong
NSF ERC for Extreme Ultraviolet Science and Technology and Department of Chemistry, Colorado State University, Fort Collins, Colorado 80523

S. Heinbuch and J. J. Rocca
NSF ERC for Extreme Ultraviolet Science and Technology and Department of Electrical and Computer Engineering, Colorado State University, Fort Collins, Colorado 80523

E. R. Bernstein[a)]
NSF ERC for Extreme Ultraviolet Science and Technology and Department of Chemistry, Colorado State University, Fort Collins, Colorado 80523

(Received 22 February 2006; accepted 12 April 2006; published online 13 June 2006)

A tabletop soft x-ray laser is applied for the first time as a high energy photon source for chemical dynamics experiments in the study of water, methanol, and ammonia clusters through time of flight mass spectroscopy. The 26.5 eV/photon laser (pulse time duration of ~1 ns) is employed as a single photon ionization source for the detection of these clusters. Only a small fraction of the photon energy is deposited in the cluster for metastable dissociation of cluster ions, and most of it is removed by the ejected electron. Protonated water, methanol, and ammonia clusters dominate the cluster mass spectra. Unprotonated ammonia clusters are observed in the protonated cluster ion size range $2 \leqslant n \leqslant 22$. The unimolecular dissociation rate constants for reactions involving loss of one neutral molecule are calculated to be $(0.6–2.7)\times 10^4$, $(3.6–6.0)\times 10^3$, and $(0.8–2.0)\times 10^4$ s^{-1} for the protonated water $(9 \leqslant n \leqslant 24)$, methanol $(5 \leqslant n \leqslant 10)$, and ammonia $(5 \leqslant n \leqslant 18)$ clusters, respectively. The temperatures of the neutral clusters are estimated to be between 40 and 200 K for water clusters $(10 \leqslant n \leqslant 21)$, and 50–100 K for methanol clusters $(6 \leqslant n \leqslant 10)$. Products with losses of up to five H atoms are observed in the mass spectrum of the neutral ammonia dimer. Large ammonia clusters $(NH_3)_n$ $(n > 3)$ do not lose more than three H atoms in the photoionization/photodissociation process. For all three cluster systems studied, single photon ionization with a 26.5 eV photon yields near threshold ionization. The temperature of these three cluster systems increases with increasing cluster size over the above-indicated ranges. © *2006 American Institute of Physics*. [DOI: 10.1063/1.2202314]

I. INTRODUCTION

The study of van der Waals cluster formation and growth in the gas phase can contribute to the understanding of solvation processes, solvation dynamics, and the nucleation and growth of small clusters. The investigation of water, methanol, and ammonia clusters together is of particular importance because these clusters demonstrate a wide range of van der Waals interactions and hydrogen bonding: water clusters are very strongly and dominantly hydrogen bonded; methanol clusters somewhat less so; and ammonia clusters perhaps not at all.[1,2]

Water clusters are one of the most important van der Waals/hydrogen bonded clusters because of their unique role in both fundamental research and a wide range of applied fields, including atmospheric science,[3,4] astrophysics,[5] and biology.[6] Neutral water clusters have been studied by electron impact (EI) ionization,[7,8] corona discharge ionization,[9,10] chemical ionization (CI),[11] vacuum ultraviolet (vuv) resonance lamp ionization,[12] and femtosecond photoionization.[13] These approaches generate mass spectra of water clusters that are typically dominated by the protonated cluster ions $(H_2O)_nH^+$: these species are produced by a fast proton transfer reaction and loss of OH from the cluster following the ionization process. The two cluster ions $(H_2O)_{21}H^+$ and $(H_2O)_{28}H^+$ are identified as "magic number" clusters in this mass spectrum since intensity anomalies of the 21-mer and 28-mer are observed under numerous experimental conditions.[14–19] The structures of medium sized protonated water clusters have been reviewed by Chang *et al.* recently.[20] Shiromaru *et al.*[12] observed unprotonated $(H_2O)_n^+$ clusters $(2 \leqslant n \leqslant 10)$ for the first time by applying near threshold photoionization with an Ar resonance lamp (11.83 eV) for a molecular beam expansion of H_2O and Ar. They suggest that unprotonated water cluster ions are generated because the mixed cluster ions $(H_2O)_n$ Ar_m^+ are created and give rise to $(H_2O)_n^+$, without sufficient excess energy needed to drive the proton transfer reaction, through evaporative loss of *m*Ar. Binding energies and metastable dissociation rate constants for protonated water clusters have been measured by Shi *et al.*[11] and Radi *et al.*[13] Water cluster mass spectra cannot be

a)Electronic mail: erb@lamar.colostate.edu

observed through nanosecond multiphoton ionization (MPI) processes because water clusters are dissociated in the MPI process.

Methanol clusters represent an important complementary class of hydrogen bonded van der Waals clusters to water clusters, as their van der Waals interaction energy should be larger and their hydrogen bonded interaction energy should be smaller than those found for water clusters. Many ionization techniques have also been employed to investigate methanol clusters (e.g., EI,[21,22] MPI,[23–25] and IR/vuv excitation[26]). As found for water clusters, protonated methanol clusters dominate the mass spectra of $(CH_3OH)_n$: unprotonated $(CH_3OH)_n^+$ $(n \leqslant 7)$ are only observable in an Ar expansion.[21] The possible relationship between methanol cluster ion distributions and methanol cluster distributions has been addressed by Shi *et al.*[27] and Fu *et al.*[26] based on single photon vuv (118 nm) laser ionization. Formation of $H^+(H_2O)(CH_3OH)_n$ and $(CH_3OH)_n[(CH_3)_2O]H^+$ clusters via two kinds of intramolecular ion-molecule reactions are observed for EI ionization,[21,22] but not for single photon (118 nm) ionization.[26,27]

Ammonia is another important solvent species: it is characterized by van der Waals, but not hydrogen bonding, interactions, as it is a very poor proton donor, albeit a very good proton acceptor [ammonia proton affinity $PA(NH_3) \sim 204$ kcal/mol (Ref. 28) vs $PA(H_2O) \sim 160$ kcal/mol (Ref. 29)]. Ammonia clusters are investigated by EI,[30,31] MPI,[32,33] femtosecond laser,[34,35] and single photoionization[36] techniques. Like water and methanol clusters, protonated ammonia clusters somewhat surprisingly dominate its mass spectra. Nonetheless, unprotonated ammonia clusters are observed by various ionization techniques.[31,35,36] Shinohara and Nishi[36] detect unprotonated ammonia cluster ions $(NH_3)_n^+$ for n up to 25 employing single photon ionization with atomic resonance lamps.

One of the more serious problems encountered in the investigation of the neutral cluster distribution of van der Waals and hydrogen bonded clusters is the fragmentation of the ionizing cluster due to intracluster ion-molecule reactions that generate protonated cluster ions. EI usually suffers considerably from the fragmentation of parent cluster ions due to the large excess (above the vertical ionization energy, VIE) energy present during the ionization process. A nanosecond MPI process results in predissociation of neutral water clusters prior to the ionization step. In general, single photon ionization is a good way to study van der Waals and hydrogen bonded clusters since less fragmentation of the parent cluster ions occurs compared to EI and MPI. We have previously demonstrated that, if 10.5 eV is sufficient energy for the ionization of a cluster,[37,38] a 118 nm vuv laser provides a nonresonant soft ionization for metal oxide and methanol clusters,[37,38] as fragmentation is minimized during the ionization process. The 10.5 eV photon, however, is not energetic enough to meet the VIE of $(H_2O)_n$.[39]

Recently, we have developed a 26.5 eV tabletop, soft x-ray laser with a 10 μJ/pulse, 10 Hz output energy that is now operational in our laboratory.[40] To the best of our knowledge, this is the first soft x-ray laser source employed to study clusters and chemical dynamics. A single photon of this laser has sufficient energy to ionize any cluster, molecule, or atom. The experimental results demonstrate that the 26.5 eV laser is a very good ionization source for many systems, including van der Waals clusters. Little photon energy remains in the cluster above the VIE following ionization, since this excess energy is removed by the ejected electron. The problem of predissociation of neutral clusters caused by MPI processes is thereby avoided.

The present study of water, methanol, and ammonia clusters is the first application of a soft x-ray laser in chemistry. Distributions of water, methanol, and ammonia clusters are compared to those found by other single photon, near threshold, photoionization techniques. Dissociation rate constants for metastable protonated water, methanol, and ammonia clusters are obtained. Temperatures of neutral clusters are estimated for water and methanol, while temperatures for ammonia clusters cannot be estimated accurately due to inconsistencies in the extant ammonia cluster data set.

II. EXPERIMENTAL PROCEDURES

The apparatus used in this experiment is shown in Fig. 1. It includes a time of flight (linear/reflectron) mass spectrometer (TOFMS) and a tabletop soft x-ray laser as an ionization source for the mass analyzer. The laser emits pulses of about 1.5 ns duration with an energy of about 10 μJ at a repetition rate of up to 12 Hz, and occupies a smaller table area than most UV gas lasers, approximately 0.4×0.4 m^2 (0.4×0.8 m^2 including a turbomolecular pump).[40(a)] The small size of this capillary discharge device is achieved by making use of a very low inductance coaxial discharge configuration illustrated in Fig. 1(b). Laser amplification is obtained for the $3p(^1S_0)-3s(^1P_1)$ line of Ne-like Ar.[40(b)] The plasma column is generated in an Al_2O_3 capillary 3.2 mm inside diameter (i.d.) and 21 cm long, filled with preionized Ar gas at an optimized pressure of 700 mTorr. The plasma column is excited by a current pulse of about 22 kA peak amplitude with a 10%–90% rise time of approximately 60 ns. The excitation current pulse is produced by discharging a set of ceramic capacitors through a pressurized spark gap switch connected in series with the capillary load. The main current pulse through the capillary is initiated by triggering the spark gap with ~50 kV pulse to allow synchronization of the laser pulse with external events with a jitter of several nanoseconds, as is required for the application of this laser as the ionization source for TOFMS experiments. The magnetic force of the current pulse and large thermal pressure gradients near the capillary wall rapidly compress the plasma to form a dense, hot column with a high density of Ne-like Ar ions, with high axial uniformity.[40(c)] Collisional electron impact excitation of the ground state Ne-like Ar ions produces a population inversion between the $3p\ ^1S_0$ and $3s\ ^1P_1$ levels of Ar^{+8}, resulting in the amplification of light at 46.9 nm (26.5 eV). The laser is described in greater detail in Ref. 40(a).

A pair of mirrors placed in a Z-fold configuration just before the ionization region of the TOFMS [Fig. 1(a)] provides alignment capability and focus for the laser beam with respect to the molecular cluster beam at the ionization

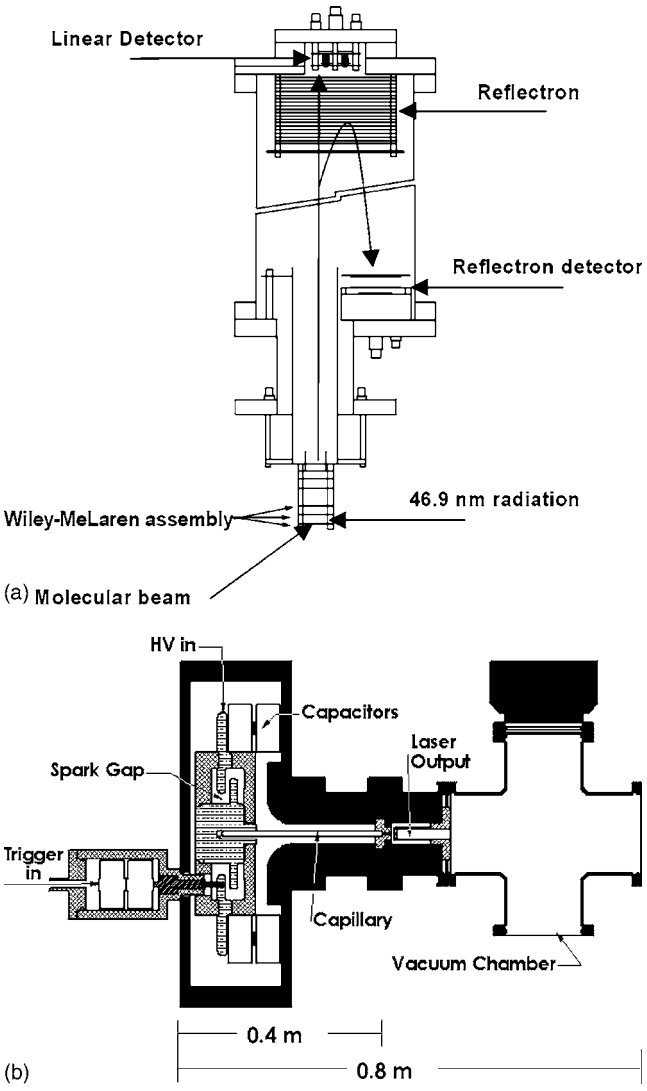

FIG. 1. (a) Schematic of the experimental setup of the reflectron time of flight mass spectrometer. (b) Schematic representation of the 46.9 nm capillary discharge, soft x-ray laser.

source. The *Z*-fold mirror set consists of two 1 in. diameter Sc/Si multilayer mirrors with about 40% reflectivity each;[41] a planar mirror, placed 30.5 cm from a $f=50$ cm concave mirror, focuses the incoming laser beam to the ionization region of the TOFMS. The use of these optics improves the experimental setup in three ways: (1) the two mirrors allow full directional control of the ionizing 46.9 nm bright beam in order to improve alignment (motor controls for the mirrors are external to the vacuum system); (2) improved intensity of the light beam at the ion source region by using a focusing mirror for a tight focal spot; and (3) a tight focal spot that results in sharp (ca. 10 ns) TOFMS features. The *Z*-fold mirror has a transmissivity of about 10% that reduces the soft x-ray laser pulse energy from ~ 10 μJ/pulse at the output of the laser to ~ 1 μJ/pulse at the entrance of the ionization region.

Neutral clusters are generated in a supersonic expansion of desired gases from a pulsed nozzle (200 μm diameter opening). During operation, saturated water or methanol vapor in He is formed by flowing He (99.9% General Air) at a pressure of 25 psi through a reservoir containing liquid distilled water or methanol (spectroscopic grade) at room temperature. The molecular beam is collimated by a 2.0 mm diameter skimmer, located approximately 2 cm downstream from the nozzle. For generation of ammonia clusters, 15% ammonia is seeded into the He carrier gas. Neutral clusters are ionized by the soft x-ray laser at 26.5 eV. For the linear time of flight (TOF) detection mode, the positive ions formed by a single photon ionization process are accelerated to 4000 eV of total kinetic energy by a three-plate Wiley-McLaren assembly (0, 3750, and 4000 V), as shown in Fig. 1(a). The accelerated ions travel 110 cm in a field-free flight tube and arrive at a microchannel plate (MCP) detector at the end of the tube. For the reflectron mode of operation, ions are accelerated by three plates (0, 700, and 1000 V) after ionization and pass through the first field-free region toward the reflection voltage grid. Ions are then reflected to travel another ~ 65 cm in a field-free region to another MCP detector [see Fig. 1(a)]. Metastable fragmentation of the ions leaving the acceleration/source region and entering the first field-free region can occur in the latter region of the TOFMS. Daughter ions generated in the first field-free region by metastable (slow, 1–100 μs) dissociation have lower kinetic energy than their parent ions but the same speed. Parents and daughters arrive at the linear TOFMS mode detector at the same flight time but can be separated in time, by adjusting the reflectron grid voltages, at the reflectron detector. Pressure in the field-free and detector regions is maintained at 2×10^{-6} Torr during the experiment. Experiments are conducted to ensure that collision induced dissociation of cluster ions is negligible.

Since the 26.5 eV photons from the soft x-ray laser are able to ionize the He carrier gas employed in the expansion, the MCP detector voltage is gated to reduce the gain of the plates when He^+ arrives at the detector in order to prevent detector circuit overload and saturation. Signals from the detector are analyzed by a 350 MHz, 5 Gs/s digitizing oscilloscope through a 50 Ω miniature high voltage (MHV) connector. Time delays between valve opening, ionization laser firing, and MCP gating are generated by two programmable Stanford Research System digital delay generators (DG 535). All timings are adjusted to maximize the spectral signal strengths.

III. RESULTS AND DISCUSSION

A. Water clusters

1. Distribution of water clusters ionized by 26.5 eV *photons*

Figure 2 displays a reflectron TOF mass spectrum of water clusters ionized by the 26.5 eV soft x-ray laser. All of the cluster features in this spectrum [except $(H_2O)_2^+$] arise from protonated water clusters of the general formula $(H_2O)_nH^+$. The parent cluster ions $(H_2O)_nH^+$ labeled by P_n in the figure are generated from the neutral species $(H_2O)_{n+1}$, ionized by the soft x-ray laser; following this event, the intracluster proton transfer reaction,

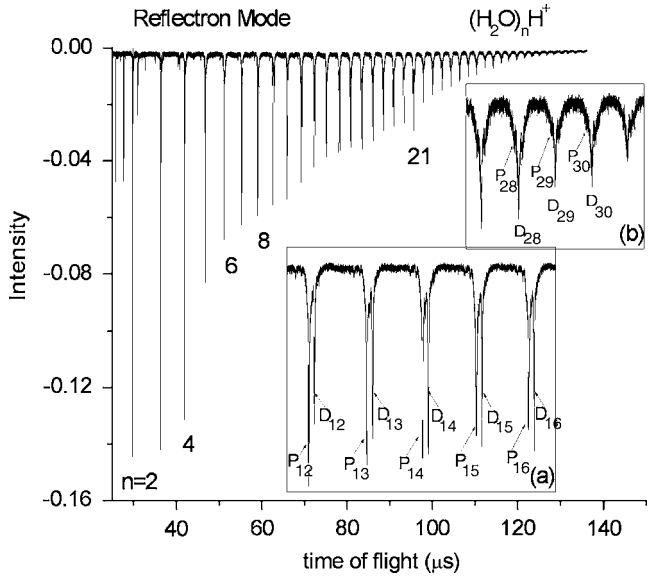

FIG. 2. A reflection TOF mass spectrum of water clusters ionized by a 26.5 eV soft x-ray laser. P_n stands for the parent ion $(H_2O)_nH$; D_n represents the daughter ion formed from P_{n+1} via losing a single water molecule in the first field-free region.

$$(H_2O)_{n+1} + h\nu \rightarrow [(H_2O)^+_{n+1}]^* + e^- \rightarrow (H_2O)_nH^+ + OH + e^-, \quad (1a)$$

is initiated. These parent ion signals dominate the mass spectrum of water clusters for small clusters up to $n=14$. This is shown clearly in the insert spectra of Fig. 2. Daughter ions labeled D_n are created from parent ions P_{n+1} by unimolecular dissociation in the first field-free region of the reflection TOFMS by the reaction

$$(H_2O)_{n+1}H^+ \rightarrow (H_2O)_nH^+ + H_2O. \quad (1b)$$

In linear mode operation, D_n and P_{n+1} appear at the same mass channel, but these two features can be separated by adjusting the reflectron grid potentials in the reflectron mode for the TOFMS. Daughter ion signals appear and dominate the mass spectral peaks in the region of larger clusters. Note that unimolecular dissociation of cluster ions is more rapid for larger clusters than smaller ones, as the D_n daughter features become larger than the P_n parent features in the spectrum. This apparent anomaly (i.e., non-RRKM behavior for clusters of a constant amount of internal energy), and the correctness of the above implicit assumption that the reaction

$$(H_2O)_n + h\nu \rightarrow (H_2O)^+_n + e^- \rightarrow (H_2O)_{n-1-m}H^+ + OH + e^- + mH_2O \quad (2)$$

does not occur rapidly (<1 ns) in the ionization region, will be discussed later in this section after more of the data are presented and discussed.

For the nine-mer cluster ion (from the ten-mer neutral cluster), the ratio of daughter ion to parent ion intensity is about 0.34. This ratio increases to about 1.0 at $n=14$. This result is in agreement with those of $(H_2O)_n$ by femtosecond MPI.[13] A distinct intensity drop occurs between peaks $(H_2O)_{21}H^+$ and $(H_2O)_{22}H^+$, as can be seen in Fig. 2, for the reflectron mode of operation of the TOFMS. The $(H_2O)_{21}H^+$

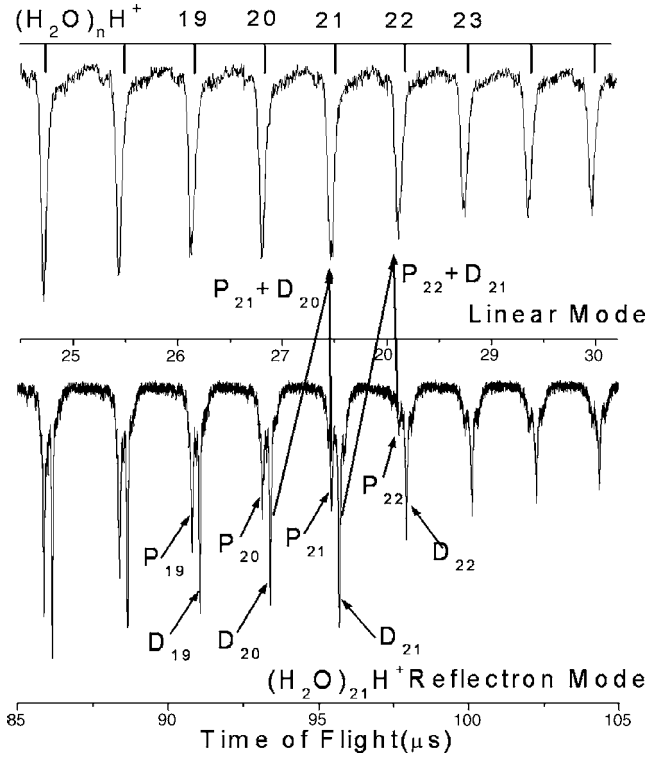

FIG. 3. Mass spectrum of size distribution of water cluster ions around the region of $n=21$. The upper spectrum is obtained by a linear mode. It reflects the distribution of the water cluster ions generated in ionization region. The lower spectrum is obtained by a reflectron mode. It shows the distribution of water cluster ions after the metastable decay in the first field-free region.

feature exhibits an enhanced intensity compared to its neighbor features. The overall $(H_2O)_nH^+$ intensity distribution also exhibits less distinct irregularities at the $(H_2O)_{28}H^+$ and $(H_2O)_{29}H^+$ features. Both $(H_2O)_{21}H^+$ and $(H_2O)_{28}H^+$ are typically suggested as magic numbers and have especially stable structures according to calculations.[42–46] These irregular intensity patterns have been supported for several different types of experiments.[14–20] Although the 26.5 eV photon energy is absorbed by a water cluster, no doubly charged species are apparent in the mass spectrum. Doubly charged water cluster ions are reported for large clusters ($n>37$) using a multiphoton (800 nm) femtosecond ionization technique.[13]

Spectra obtained by the two TOFMS modes of operation are compared in Fig. 3. The upper spectrum is obtained in the linear TOFMS mode: it records the size distribution for cluster ions created in the acceleration region, approximately within less than 1 μs following single photon 26.5 eV ionization. Note that this ion intensity decreases roughly exponentially and smoothly as a function of cluster size n. No obvious intensity anomaly at $(H_2O)_{20}H^+$ generated from $(H_2O)_{21}$ ionization is observed. This indicates that the neutral cluster $(H_2O)_{21}$ does not enhance the intensity of its "daughter" protonated $(H_2O)_{20}H^+$ cluster in the distribution of protonated cluster ions. Thus the neutral cluster distribution in the beam is roughly exponentially decreasing as a function of cluster size n.

The lower spectrum in Fig. 3 is obtained with the TOFMS operated in the reflectron mode. This spectrum in-

dicates the population distribution of cluster ions formed in the first field-free region within the time range of 1–80 μs. A strong intensity decrease for the parent cluster ion P_{22}, $(H_2O)_{22}H^+$, and an obvious intensity enhancement at daughter ion D_{21}, $(H_2O)_{21}H^+$, which derives from the reaction

$$(H_2O)_{22}H^+(P_{22}) \rightarrow (H_2O)_{21}H^+(D_{21}) + H_2O$$

can be readily discerned. Note that P_{21} is not significantly more intense than P_{20} in Fig. 3. Similarly, the daughter ion of P_{21}, D_{20}, is not significantly smaller than other neighbor daughter ions, such as D_{19}. D_{21} appears to be the most intense feature in this mass region. This set of intensities indicates that the parent ion P_{21} [created from $(H_2O)_{22}$ ionized by 26.5 eV photon] does not evidence an especially stable structure even though calculations suggest enhanced stability for P_{21}.[42–46] Collecting and organizing all these facts lead one to the conclusion that the intensity anomalies ca. $n=21$ are due to the unstable behavior of the metastable parent ion P_{22}, $(H_2O)_{22}H^+$, which arises from the neutral cluster $(H_2O)_{23}$ in the molecular beam. The parent ion P_{22}, $(H_2O)_{22}H^+$, dissociates rapidly in the field-free region yielding an enhanced signal intensity for D_{21}, its daughter species.

Echt *et al.*[7] also observed a similar behavior employing EI ionization at 40 eV in a linear mode TOFMS. In their experiment, a positive voltage was applied to a barrier grid in front of the detector to block daughters from reaching the detector. This was accomplished because, while daughter ions have nearly the same velocity as parent ions in the field-free region between the acceleration region and the linear mass detector, they have lower kinetic energy. They found that the parent P_{22} ion intensity is much lower than its neighbors $(H_2O)_{21}H^+$ (P_{21}) and $(H_2O)_{23}H^+$ (P_{23}). The conclusion is that the parent ion P_{22} dissociates rapidly after leaving the acceleration region of the TOFMS. On the other hand, if no positive potential barrier is placed in front of the mass detector (that is, parent and daughter ions are simultaneously detected at the same mass channel-time), the distribution of protonated cluster ions decreases roughly exponentially with increasing cluster size. The implication of these results is that the neutral cluster distribution evidences no anomalies. Thus both the present data and those of Ref. 7 reach the same conclusions, implying that 40 eV EI and 26.5 eV single photon ionization yield the same cluster ion distribution based on the same neutral cluster distribution.

2. Observation of neutral water dimer

As shown in Fig. 4(a), a small signal for $(H_2O)_2^+$ is observed on the low mass side of $(H_2O)_2H^+$, the daughter ion for $(H_2O)_3$. In general, unprotonated water clusters are not observed in our experiments, in which He is employed as the backing/expansion gas. Most of the neutral dimers in the beam generate $(H_2O)H^+$ ions following single photon ionization by 26.5 eV photons. If 5% Ar is mixed into the He expansion gas, the $(H_2O)_2^+$ signal increases and the H_3O^+ signal decreases [see Fig. 4(b)]. For a 20% Ar/80% He expansion, the $(H_2O)_2^+$ mass feature is much larger than that for H_3O^+ [Fig. 4(c)]. The intensity of the protonated cluster ion $(H_2O)_2H^+$ also decreases as Ar concentration in the binding gas is increased.

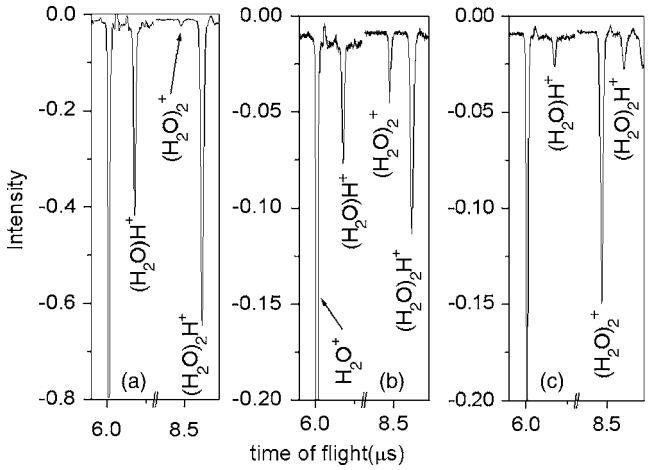

FIG. 4. TOF mass spectra of unprotonated water dimer ion formed in different carrier gases: (a) pure He gas, (b) 5% Ar mixed in He gas, and (c) 20% Ar mixed in He gas, respectively.

Ng *et al.*[29] measured the appearance potentials for H_3O^+ and $(H_2O)_2^+$ as 11.73 and 11.21 eV, respectively. Shiromaru *et al.*[12] observed various unprotonated water cluster ions $(H_2O)_n^+$ $(2 \leqslant n \leqslant 10)$ by photoionization of neutral $(H_2O)_n$ with atomic vuv resonance lines at 11.83 and 11.63 eV. They explain that unprotonated ions are produced from mixed $Ar_n(H_2O)_m^+$ cluster ions followed by the loss of Ar through evaporation. They also observe that 40 eV EI ionization does not yield $(H_2O)_n^+$ signals. Nonetheless, Shiromaru *et al.*[47] observe $(H_2O)_n^+$ $(1 \leqslant n \leqslant 6)$ cluster ions ionized by synchrotron radiation at 85 nm (14.6 eV) for the $Ar/H_2O/He$ system. This photon energy is ca. 3 eV larger than that employed with Ar resonance lamps and certainly enough excess energy above the VIE of $(H_2O)_n^+$ to induce intracluster proton transfer and form $(H_2O)_{m-1}H^+$. They suggest that the unprotonated water clusters are generated because most of the excess energy following single photon ionization is removed from the cluster by the exiting electron.

Single photon ionization by a 26.5 eV photon has also much more energy (ca. 15 eV) than that required for ionization of all the water clusters. If this energy were to remain in the clusters, we would observe only H_2O^+ and its fragments in our TOFMS. Nonetheless, $(H_2O)_2^+$ is observed in this experiment even with no Ar present in the expansion. Again this suggests that almost all of the excess energy in these clusters (ca. 15 eV) is removed by the exiting electron. Single photon ionization of water clusters thus seems to be very gentle in terms of fragmentation even with a 26.5 eV photon.

In the preceding presentation of results and discussion, dissociation of protonated water cluster ions, directly following the ionization of neutrals in the ion source/extraction region of the TOFMS, is assumed not to occur. The loss of at most only one water molecule for each cluster $(H_2O)_nH^+$ (created by ionization, rapid proton transfer, and loss of OH) through metastable dissociation occurs only in the flight tube (1–2 μs after ionization). While this assumption cannot be proven by our data or that of others, the following four observations can be collected to support this assumption. First, the linear mode TOFMS reflects the size distribution of clus-

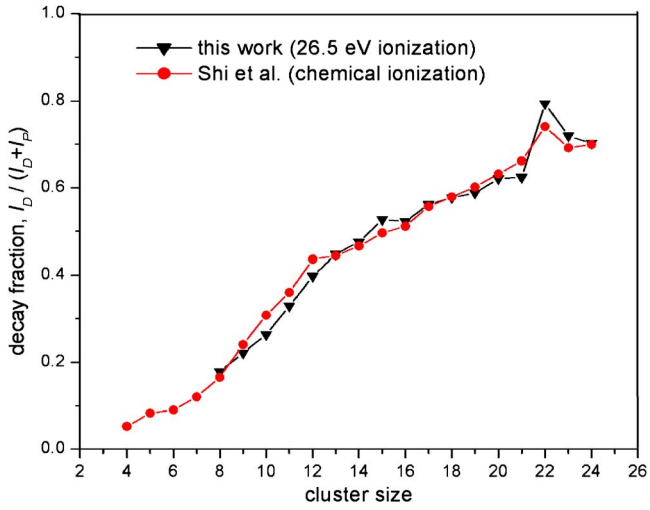

FIG. 5. Decay fractions of protonated water clusters $(H_2O)_nH^+$, as a function of cluster size n (Ref. 11).

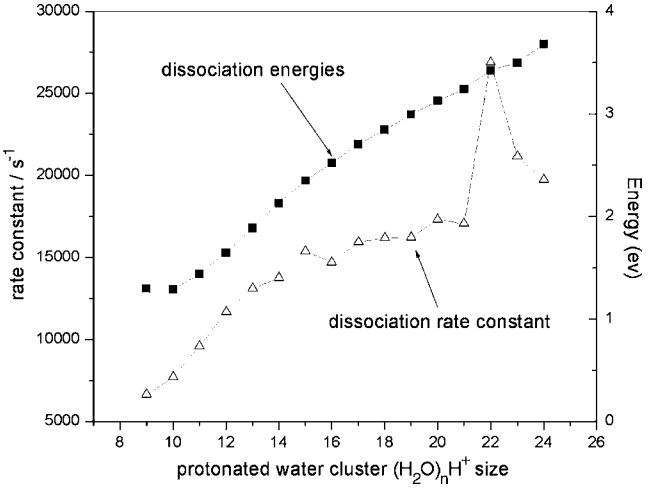

FIG. 6. Metastable dissociation rate constants and dissociation energies for protonated water clusters.

ter ions formed within the acceleration/extraction region of the TOFMS, approximately less than 1 μs following ionization (see Fig. 3). The individual features of cluster ions $(H_2O)_nH^+$ $17 \leqslant n \leqslant 25$ can be fitted to a Gaussian curve. If metastable dissociation of cluster ions $(H_2O)_nH^+$ were to occur in less than 1 μs, a long tail should be observed on each cluster feature in the linear mass spectrum to the high mass, long time side of each peak. Second, one knows that the intensity of the mass peak for $(H_2O)_{21}H^+$ is due to the fast metastable dissociation of the $(H_2O)_{22}H^+$ cluster ion. If metastable dissociation of $(H_2O)_{22}H^+$ occurs in the acceleration/extraction region of the TOFMS, an enhanced intensity of $(H_2O)_{21}H^+$ should be observed in the linear mode TOFMS, as the linear spectrum reflects the cluster ion distribution formed within this region. As shown in Fig. 3, this is not the case. Nonetheless, an enhanced intensity is clearly observed for $(H_2O)_{21}H^+$ in the reflectron TOFMS (Fig. 3), proving the metastable fragmentation of $(H_2O)_{22}H^+$ to generate $(H_2O)_{21}H^+$ occurs in the flight tube at times between $\sim$1 and $\sim$100 μs. Only the loss of one monomer is observed in the reflectron TOFMS of water clusters. Third, based on studies of cluster ion metastability, the unimolecular decay occurs within a time window of 1–15 μs for these cluster ions.[11,48] This additionally holds true for methanol,[23] ammonia,[49] and acetone (Ref. 50) cluster ions. Fourth, if very rapid cluster ion fragmentation was to occur in the ionization/acceleration/extraction region of the TOFMS for all the clusters, at least some of the cluster ions should show such behavior as a function of size, and more complex line shapes and cluster populations should be apparent in either linear or reflectron TOFMS operation.

3. Dissociation rate constants for metastable water cluster ions

Unimolecular dissociation of metastable protonated water clusters can be observed during the time window from $\sim$1 to $\sim$80 μs, corresponding to the flight time in the first field-free region of the reflectron TOFMS. The decay fractions, $I_D/(I_D+I_P)$, for clusters have been obtained (Fig. 5) in which I_D and I_P are the integrated intensities of the daughter and parent ions, respectively. An obvious increase in the decay fractions occurs at $n=22$, and this fraction decreases slightly at $n=21$. These results show good agreement with observations reported by Shi *et al.*[11] using chemical ionization. Both our results and those of Shi *et al.* are plotted in Fig. 5.

The unimolecular dissociation rate constant for protonated water cluster ions can be obtained from these decay fractions. The rate constant k can be represented as

$$k = -\left(\frac{1}{t}\right)\ln\left[1 - \frac{I_D}{I_D + I_P}\right] = -\frac{1}{t}\ln\left[\frac{I_P}{I_D + I_P}\right], \qquad (3)$$

in which t is the flight time of the parent ion in the first field-free region of the reflectron TOFMS. For the present apparatus, this flight time is about 60% of the total reflectron flight time shown in the reflectron TOFMS of Fig. 2. Rate constants for the metastable dissociation of parent cluster ions to daughter cluster ions are found to be in the range of $(0.6–2.7)\times 10^4$ s^{-1} within the cluster ion size range of $9 \leqslant n \leqslant 24$, as plotted in Fig. 6. An obvious increase in the dissociation rate constant occurs for k_{22}. These rate constants are in agreement with those reported using femtosecond ionization:[13] for $8 \leqslant n \leqslant 18$, k_n falls in the range of $(0.8–1.3)\times 10^4$ s^{-1}. This correspondence further suggests that the assumed fragmentation behavior [loss of only one water molecule following the proton transfer reaction to generate $(H_2O)_nH^+$ cluster ions, which occurs slowly in the first field-free region of the reflection TOFMS] is correct.

An obvious decrease in cluster ion intensity occurs at P_{22} in the parent ion distribution and an increase in cluster intensity occurs at D_{21} in the daughter ion distribution (see Fig. 3). This behavior is caused by the fast dissociation of protonated water clusters at P_{22}, $(H_2O)_{22}H^+$: thus the $n=21$ cluster ion has been termed a "magic number." Suggestions have been made that this enhanced cluster stability at $n=21$ is due to a stable dodecahedral cage structure of the protonated $(H_2O)_{21}H^+$.[42–46] An anomalously small dissociation rate of parent $(H_2O)_{21}H^+$ compared to its neighbor parent cluster ions is not observed, however. We find no clear evidence in

TABLE I. Data used to calculate the temperature of neutral water clusters in the molecular beam.

n	E_{disso} (eV)[a] $(H_2O)_{n-1}H^+$	$-\Delta_a H_{n-1,n}$ (eV)	$-\Delta_b H_{n,n+1}$ (eV)[c]	ΔH_n (eV)[d] $(H_2O)_n$	E_{excess} (eV)[e] $(H_2O)_{n-1}H^+$	E_{therm} (eV)[f] $(H_2O)_n$	Temp. (K) $(H_2O)_n$
2		1.409	0.456	11.73			
3		0.872	0.529	10.777			
4		0.759	0.383	10.435			
5		0.581	0.356	10.059			
6		0.520	0.454	9.834			
7		0.464	0.697	9.768			
8		0.522	0.391	10.002			
9		0.424	0.497	9.871			
10	1.298	0.381	0.259	9.943	1.057	0.242	47
11	1.290	0.386	0.622	9.822	1.178	0.112	20
12	1.441	0.404	0.445	10.058	0.940	0.500	79
13	1.647	0.426	0.495	10.099	0.898	0.749	109
14	1.886	0.447	0.369	10.168	0.830	1.056	142
15	2.126	0.460	0.466	10.090	0.907	1.219	152
16	2.347	0.465	0.439	10.096	0.901	1.446	169
17	2.519	0.470	0.540	10.070	0.927	1.592	174
18	2.705	0.467	0.368	10.140	0.856	1.848	190
19	2.843	0.467	0.529	10.040	0.955	1.888	184
20	2.992	0.457	0.446	10.103	0.892	2.100	193.
21	3.127	0.458		10.092	0.908	2.219	194

[a]Calculated based on dissociation rate constant obtained in the present experiment.
[b]Taken from experimental data of Ref. 11 and webbook.nist.gov.
[c]Taken from theoretical calculations of Refs. 53 and 54.
[d]Calculated from the thermodynamic cycles displayed in Fig. 8.
[e]$E_{\text{excess}}=\text{VIP}(11.0\text{ eV})-\Delta H_n$.
[f]$E_{\text{therm}}=E_{\text{dissoc}}-E_{\text{excess}}$.

our experiments to document that $(H_2O)_{21}H^+$ is more stable than other cluster ions. Based on our observations we conclude that the magic number at $n=21$ is due to the enhanced dissociation rate of parent ion $(H_2O)_{22}H^+$ to its daughter ion $(H_2O)_{21}H^+$ (i.e., $P_{22}\rightarrow D_{21}+H_2O$).

The energy required for metastable unimolecular dissociation of parent ion clusters in the field-free drift tube can be calculated employing the classical RRK theory,[51]

$$k=\nu(1-E_{\text{bind}}/E_{\text{dissoc}})^{s-1}, \tag{4}$$

in which $E_{\text{activation}}$ is replaced by E_{bind} of protonated water clusters. One assumes here that no barriers to dissociation exist for this process; that is, $E_{\text{activation}}\sim E_{\text{bind}}$. Values of E_{bind} are taken from Ref. 11. The ensuing rate constants k are illustrated in Fig. 6. A value of $\nu=10^{13}$ s^{-1} is taken for the intermolecular vibrational coordinate frequency for the dissociative reaction coordinate. Assuming that only intermolecular degrees of freedom participate in the dissociation of $(H_2O)_nH^+$ to $(H_2O)_{n-1}H^+ + H_2O$ in the field-free region, $S=6n-6$. Water has three internal vibrational modes 3675, 3756, and 1595 cm^{-1}.[66] For large clusters these molecular modes also make a contribution to dissociation due to fast internal transfer of vibrational energy. Based on the heat capacity of water clusters, Ref. 11 suggests that $C_n=(6.6n-6)k_B$ for $6\leqslant n\leqslant 29$, and thus with $E=C_nT$, $S=(6.6n-6)$ is reasonable for RRK calculations of k for water clusters. Similar results are obtained for ammonia clusters.[52] E_{dissoc} for the unimolecular reaction $P_n\rightarrow D_{n-1}+H_2O$ is also given in Fig. 6 and Table I. The dissociation energy does not change much at $n=22$ (P_{22}), although the k_{22} rate constant for the loss of H_2O at $n=22$ is much larger than that of other clusters, due to the exponential relation for $k\propto E^S$ given in Eq. (4).

4. Vibrational temperature of water clusters

Neutral water clusters are ionized by absorption of a 26.5 eV single photon. If all the photon energy is used to ionize and subsequently dissociate the clusters, they will, however, for large n, fragment in single H_2O molecules. This point is, in fact, the main reason we explore the behavior of van der Waals and hydrogen bonded clusters with respect to the 26.5 eV single photon ionization. Nonetheless, the water cluster ion distribution appears in the TOFMS, and even the unprotonated dimer is observed (see Fig. 4). One can thus reasonably assume that almost all the photon energy above the VIE is removed from the cluster by the exiting photoelectron. This assumption is also suggested by Ref. 47 based on observed unprotonated water clusters ($2\leqslant n\leqslant 6$) in an Ar carrier gas using 85 nm (14.6 eV) ionization. *Ab initio* calculation of the VIEs of water clusters ($n=2-8$) show that VIEs decrease with increasing cluster size n and appear to converge ca. 11.0 eV. We thereby suggest that for neutral cluster ionization by 26.5 eV photons a photon energy above ~11.0 eV is removed by the exiting photoelectron for clusters $9\leqslant n\leqslant 24$. Part of the deposited photon energy in the neutral cluster $(H_2O)_n$ must be used to initiate the proton transfer reaction $[(H_2O)_{n+1}\rightarrow(H_2O)_nH^+(P_n)+OH]$ and the following unimolecular dissociation of the protonated cluster $[(H_2O)_nH^+(P_n)\rightarrow(H_2O)_{n-1}H^+(D_{n-1})+H_2O]$. If we neglect

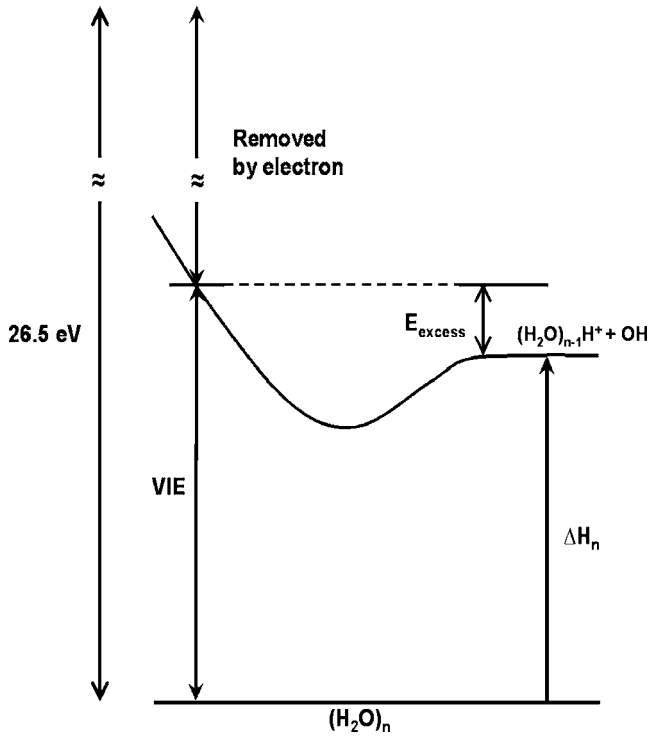

FIG. 7. Schematic of the potential energy diagram for ionization of water clusters. 26.5 eV photon energy is absorbed by a neutral water cluster, $(H_2O)_n$. The photon energy above VIE is removed by an electron. ΔH_n is the minimum energy to initiate the reaction of $(H_2O)_n \rightarrow (H_2O)_{n-1}H^+ + OH$. Excess energy ($E_{excess}$) comes from a soft x-ray laser photon to be used for metastable dissociation of $(H_2O)_{n-1}H^+$.

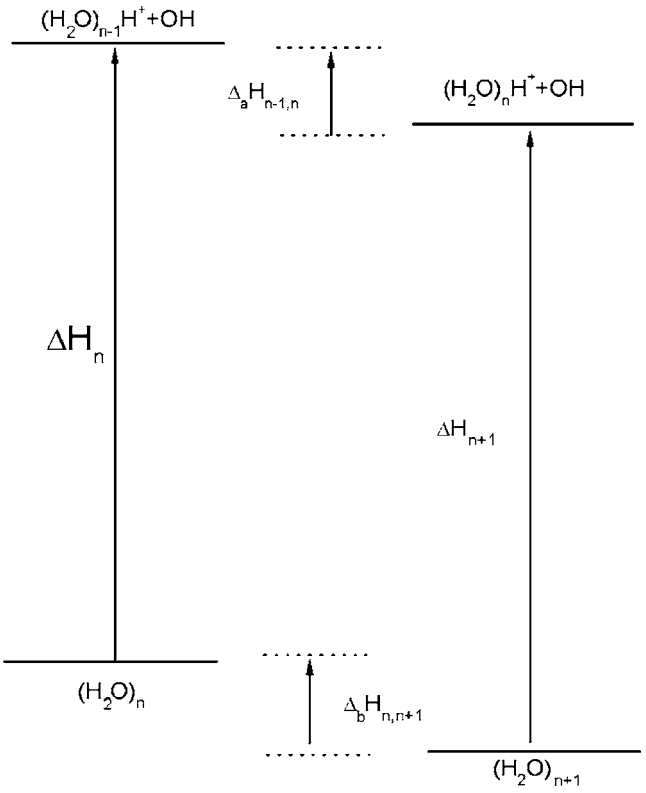

FIG. 8. Thermodynamic energy diagram for water clusters.

the transitional energy release of the fragments, the excess energy (E_{excess}) that comes from a soft x-ray laser photon and is used for metastable dissociation of $(H_2O)_nH^+$ can be determined.

As shown in Fig. 7, the excess energy is the difference between the VIE ($\sim$11.0 eV) of a water cluster and the reaction energy (ΔH_n) of $(H_2O)_n \rightarrow (H_2O)_{n-1}H^+ + OH + e^-$. Thus $E_{excess} = (\text{VIE}(11.0\ \text{eV}) - \Delta H_n)$, with ΔH_n for cluster sizes $9 \leqslant n \leqslant 22$ calculated based on the thermodynamic cycle shown in Fig. 8. $\Delta_a H_{n-1,n}$ is the reaction energy of a protonated cluster $(H_2O)_{n-1}H^+$ combined with a water molecule to generate $(H_2O)_nH^+$. This value can be obtained from the experimental data of Ref. 11. $\Delta_b H_{n,n+1}$ is the reaction energy of the neutral cluster $(H_2O)_n$ combined with another water molecule. This value is obtained from calculations.[53,54] Thus the following relation can be obtained:

$$\Delta H_{n+1} = \Delta H_n + \Delta_a H_{n,n-1} - \Delta_b H_{n,n+1}. \quad (5)$$

The appearance energy of H_3O^+ is measured as 11.73 eV (Ref. 29) and the ΔH_2 of the dimer reaction is known as

$$(H_2O)_2 \rightarrow (H_2O)H^+ + OH, \quad \Delta H_2 = 11.73\ \text{eV}. \quad (6)$$

Given Eq. (6) $\Delta H_3, \Delta H_4, \ldots$, can be calculated. ΔH_n is the minimum energy required for initiation of the reaction $(H_2O)_n \rightarrow (H_2O)_{n-1}H^+ + OH + e^-$ without excess energy used for metastable dissociation of the protonated cluster, $(H_2O)_{n-1}H^+$. These ΔH_n values are listed in Table I.

Through comparison of the dissociation energy (E_{dissoc}) calculated based on experimental data and the excess energy (E_{excess}) that is deposited by the soft x-ray laser photon upon ionization, one finds that $E_{excess} < E_{dissoc}$, implying that just E_{excess} is insufficient to dissociate the metastable cluster ion at the experimentally determined rate. The required E_{dissoc} for the metastable cluster ion can come from two sources. One source is E_{excess} from the ionization photon (listed in Table I). Another source is the internal thermal vibrational energy of the neutral cluster, which depends on cluster temperature in the molecular beam. The cluster thermal energy can thus be calculated by the relation $E_{therm} = E_{dissoc} - E_{excess}$, as listed in Table I.

Based on a thermodynamic mechanism, k_BT is the thermal (statistical) energy associated with each degree of freedom for the cluster. The vibrational energy contribution to the total cluster available energy is $E_{therm} = k_BT\ (6.6n - 6)$. The temperatures of neutral water clusters can thus be estimated within this classical approximation. As shown in Table I they are in the range of 40–200 K for clusters $10 \leqslant n \leqslant 21$. The higher temperatures of larger clusters with respect to smaller ones are due to the exothermic reaction of added water molecules to the neutral clusters. This must be true if the RRK calculated dissociation rate constant k_n increases rather than decreases with increasing cluster size. The results in Table I for T_n give $T_{11} < T_{10}$ because the reaction energy for $n = 10$ ($\Delta_b H_{10,11} = -0.259$ eV) is lower than that for $n = 11$: this result gives $\Delta H_{10} > \Delta H_{11}$. In addition, perhaps the VIEs of all water clusters ($9 \leqslant n \leqslant 21$) are not truly constant at 11.0 eV, especially near the small cluster end of this range.

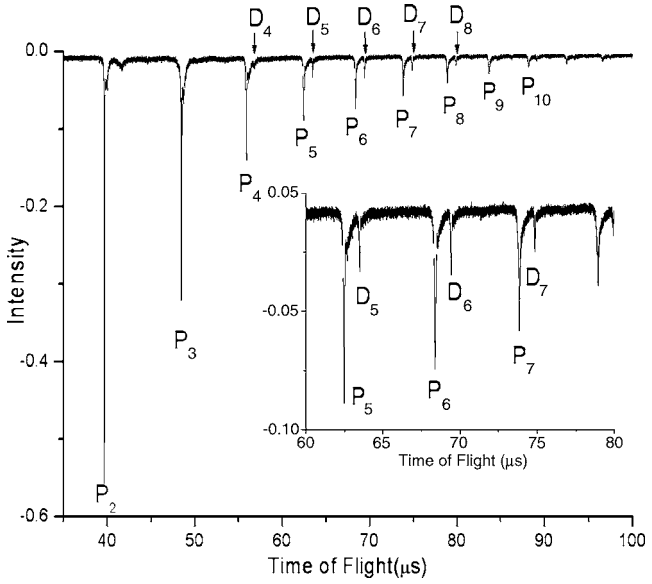

FIG. 9. A reflectron TOF mass spectrum of methanol clusters photoionized by a 26.5 eV soft x-ray laser. The peaks labeled P_n correspond to parent ion series. The peaks labeled D_n belong to the daughter ion series, which is formed via loss of CH_3OH from parent ions P_{n+1}.

B. Methanol clusters

1. Distribution of methanol clusters ionized at 26.5 eV

The reflectron TOFMS of methanol clusters ionized by 26.5 eV photons is shown in Fig. 9. Two major series of ion peaks are observed: the protonated $(CH_3OH)_nH^+$ (P_n parent ions) and their daughter ion peaks $(CH_3OH)_{n-1}H^+$ (D_{n-1}). The protonated parent ions are generated from the neutrals by a rapid internal ion-molecule reaction as follows:

$$(CH_3OH)_n + h\nu \rightarrow [(CH_3OH)_n^+]^* + e^- \rightarrow (CH_3OH)_{n-1}H^+ + CH_3O + e^-. \quad (7)$$

Daughter ions are generated in the field-free flight tube at longer times (ca. 1–80 μs) by the loss of one CH_3OH molecule,

$$(CH_3OH)_{n-1}H^+ \rightarrow (CH_3OH)_{n-2}H^+ + CH_3OH. \quad (8)$$

In our single photon 26.5 eV ionization approach, only one (CH_3OH) is lost by the parent cluster ion. (See the discussion for the water clusters concerning this point.) In MPI experiments,[23,25] loss of up to five methanol monomers from the protonated octomer is observed. Ions corresponding to unprotonated clusters, $(CH_3OH)_n^+$ ($n>2$), are not generally detected employing a pure He expansion. Vaidyanathan *et al.*[21] observed unprotonated cluster ions ($n\leqslant 7$) in an Ar expansion, as has been observed for water clusters (see above and Ref. 12). They suggest that in this instance and with ionization by low energy electron impact ($\leqslant$20 eV), such species can be attributed to indirect ionization of neutral heteroclusters of the form $Ar_m(CH_3OH)_n$ via intracluster Penning ionization. A similar behavior is also observed by Shiromaru *et al.*[12] and Shinohara *et al.*[65] for water and ammonia clusters. The soft x-ray laser generated mass spectrum shows no intensity peak anomalies and the intensity of $(CH_3OH)_nH^+$ features is smoothly decreasing with increasing n. Similar results are obtained for EI,[21,22] 118 nm,[26,27] and MPI (Refs. 23–25) studies of the methanol cluster system.

Some studies[22,26,27] have found that the protonated trimer ion $(CH_3OH)_3H^+$ is more intense than the protonated dimer feature, while others[21,23–25] have not. The present results show $(CH_3OH)_2H^+$ to be more intense than $(CH_3OH)_3H^+$ by roughly 60% (see Fig. 9). This is not due to the fragmentation of larger clusters by 26.5 eV ionization in the ionization/acceleration region as the protonated dimer feature is narrower than the larger cluster features including the protonated trimer. In these experiments $(CH_3OH)_2H^+$ is not fragmented from larger clusters and we suggest that the observed intensity distribution represents (but clearly is not identical to) the neutral methanol cluster distribution in the molecular beam. Arguments against rapid wholesale fragmentation of neutrals in the ionization region have been offered for water clusters and a similar set of reasons can be offered in this instance against such an occurrence. The 118 nm ionization results,[26,27] which give a protonated dimer ion signal smaller than the protonated trimer ion signal, can be explained as due to a near threshold ionization of the neutral trimer leading to a reduced cross section for ionization. The reduced ionization cross section near threshold can be associated with a poor Franck-Condon overlap between the neutral and ionic methanol trimers.

Another series of cluster ions is observed in EI (Refs. 21 and 22) and MPI (Refs. 23 and 24) experiments. These clusters are identified by the empirical formula $(CH_3OH)_nH_3O^+$ for $n\geqslant 7$. The suggested product generation mechanism is

$$(CH_3OH)_nH^+ \rightarrow (CH_3OH)_{n-2}(H_2O)H^+ + (CH_3)_2O. \quad (9)$$

This series of clusters is not observed by either 10.5 (Ref. 26) or 26.5 eV single photon ionization. Reaction (9) requires roughly 2 kcal/mol more activation energy than reaction (8) in order to occur[22] for $(CH_3OH)_nH^+$, $n\geqslant 3$. For near threshold 118 nm (10.5 eV) ionization one can assume that the $(CH_3OH)_nH^+$ cluster ions do not have sufficient activation energy for the reaction (9) channel to be open. The reason that 26.5 eV ionization does not generate reaction (9) is most probably the same: excess energy above the VIE for those clusters is removed by the exiting electron, as is found above for water clusters.

A weak feature is observed (Fig. 10) at $m/z=47$ and is assigned as $(CH_3)_2OH^+$. This feature probably arises from the methanol dimer as follows:[55]

$$(CH_3OH)_2H^+ \rightarrow (CH_3)_2OH^+ + H_2O, \quad \Delta H = 22.7 \text{ kcal/mol}. \quad (10)$$

The $(CH_3)_2OH^+$ ion is also observed by MPI (Refs. 23 and 24) and EI,[21,22] but not by 118 nm ionization.[26,27] Again the suggestion is that near threshold ionization (118 nm) and, in general, single photon (46.9 nm) ionization do not leave sufficient energy in the protonated dimer ion (neutral timer) to open reaction channel (10). Reaction (8) has a lower activation energy than either (9) or (10).

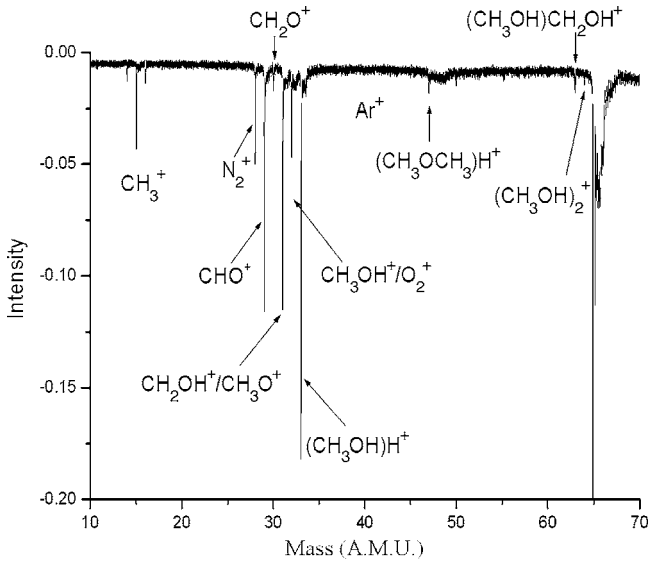

FIG. 10. Mass spectrum of methanol monomer and dimer ionized by a 26.5 eV soft x-ray laser.

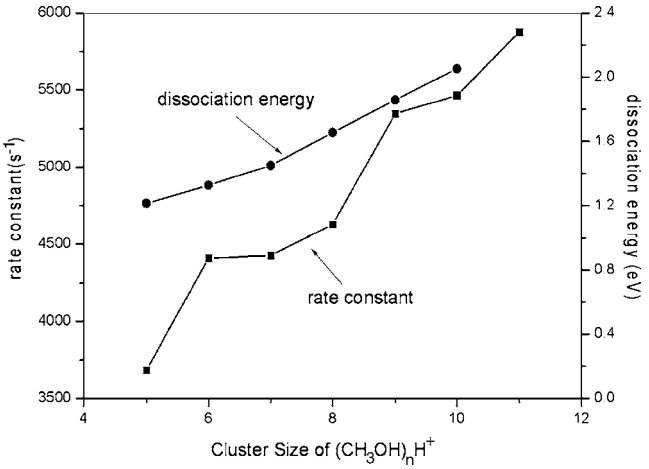

FIG. 11. Metastable dissociation rate constants and dissociation energies for protonated methanol clusters.

2. Photolysis of methanol monomer and dimer

Figure 10 depicts the mass spectrum of the methanol monomer and dimer ionized by 26.5 eV photons. The products CH_3^+, CHO^+, CH_2O^+, CH_2OH^+/CH_3O^+, and CH_3OH^+ are observed from the photolysis of the CH_3OH molecule. The product channels are thus

$$CH_3OH + h\nu \rightarrow CH_3OH^+ \quad 20.2\% \tag{11a}$$

$$\rightarrow CH_3^+ + OH \quad 12.5\% \tag{11b}$$

$$\rightarrow CHO^+ + H_2 + H \quad 31.5\% \tag{11c}$$

$$\rightarrow CH_2OH^+/CH_3O^+ + H \quad 31.2\% \tag{11d}$$

$$\rightarrow CH_2O^+ + H_2 \quad 4.6\%\,. \tag{11e}$$

The CHO^+ and CH_2OH^+/CH_3O^+ are the major photolysis channels, with the undissociated methanol ion channel yielding about 20% of the product species. CH_3OH^+ is not observed for MPI,[23,24] as either predissociation occurs before ionization or ionization occurs at very high internal methanol excess energy.

An additional minor feature associated with the methanol dimer appears at the $(CH_3OH)CH_2OH^+$ mass channel, as shown in Fig. 10. Similar ions are not observed for larger clusters. One possible reason for the rich ion chemistry for CH_3OH and $(CH_3OH)_2$, but not $(CH_3OH)_n$, $n>2$, is that for these two species the VIE can be much larger than the adiabatic ionization energy (AIE) and thus the ionization process generates more excess energy in these two small species than it does for larger clusters.

3. Dissociation rate constant of metastable methanol cluster ions

The unimolecular dissociation rate constant for the loss of one CH_3OH from the cluster $(CH_3OH)_nH^+$ can be obtained from the decay fraction of the parent cluster P_n. The approach employed here is the same as that employed to analyze the decay rate of water cluster ions. As shown in Fig. 11, the dissociation rate constants are in the range of $(3.6-6.0)\times 10^3\ s^{-1}$ for methanol cluster ion sizes $5 \leqslant n \leqslant 11$. Compared with the results of MPI experiments,[25] the rate constants obtained are ~2–3 times smaller. These rates again suggest that MPI deposits more energy into the neutral methanol clusters than does single photon ionization, even at 26.5 eV, which is ca. 15 eV above the cluster VIE. This point is also documented by the absence of product cluster ions such as $(CH_3OH)_nH_3O^+$ [observed by MPI (Refs. 23 and 24) and EI (Refs. 21 and 22) studies].

Based on the dissociation rate constant for $(CH_3OH)_nH^+ \rightarrow (CH_3OH)_{n-1}H^+ + CH_3OH$, the dissociation energy (E_{dissoc}) required for the unimolecular (statistical RRK) dissociation of protonated methanol cluster ions can be calculated. The values for $E_{bind,n}$ are taken from Ref. 56. The rate constants are shown in Fig. 11. The methanol molecule has two vibrational modes whose energies[66] (295 and 200 cm^{-1}) are very close to those for the cluster van der Waals modes: we thus let $S=8n-6$, and $E_{dissoc,n}$ can be obtained as listed in Table II and plotted in Fig. 11. More energy is required for unimolecular dissociation of larger clusters, since these clusters have a larger number of vibrational states in which to store energy than do smaller ones. Note that the larger clusters dissociate faster than the smaller ones: this is not a statistical (ergodic) result if the clusters are considered to have a constant amount of energy based on VIE and reaction energies. This is, of course, the same trend as found for water clusters above.

4. Vibrational temperature of neutral methanol clusters

The distribution of protonated methanol cluster ions obtained by 26.5 eV ionization is about the same as that observed for 10.5 eV ionization except for the protonated dimer ion intensity. Apparently all the energy above the VIE of methanol clusters is removed by the photoejected electron. This point has also been documented above for water clusters. If product translational energy release is neglected, the excess energy (E_{excess}) due to x-ray laser photon absorption

TABLE II. Data used to calculate the vibrational temperature of neutral methanol clusters in the molecular beam.

n	E_{dissoc} (eV)[a] $(CH_3OH)_{n-1}H^+$	$\Delta_a H_{n-1,n}$ (eV)[b]	$\Delta_b H_{n,n+1}$ (eV)[c]	ΔH_n (eV)[d] $(CH_3OH)_n$	E_{excess} (eV)[e] $(CH_3OH)_{n-1}H^+$	$E_{thermal}$ (eV)[f] $(CH_3OH)_n$	Temp. (K) $(CH_3OH)_n$
2		1.435	0.416	10.58			
3		1.14	0.674	9.56			
4		0.698	0.567	9.09			
5		0.585	0.532	8.96	0.94		
6	1.213	0.542	0.442	8.91	0.99	0.223	62
7	1.326	0.516	0.468	8.81	1.09	0.236	55
8	1.451	0.52	0.473	8.76	1.14	0.311	62
9	1.655	0.52	0.492	8.71	1.19	0.465	82
10	1.857			8.69	1.21	0.647	102
11	2.052						

[a]Calculated based on dissociation rate constant obtained in the present experiment.
[b]Taken from experimental data of Ref. 56.
[c]Taken from theoretical calculations of Ref. 57.
[d]Calculated based on the same thermodynamic cycles employed for the water cluster in Fig. 8.
[e]$E_{excess}=\mathrm{VIP}(9.9\ \mathrm{eV})-\Delta H_n$.
[f]$E_{therm}=E_{dissoc}-E_{excess}$.

by the cluster that is used for the metastable dissociation of $(CH_3OH)_nH^+$ can be calculated (as discussed above for the water cluster system) as

$$E_{excess}=\mathrm{VIE}-\Delta H_n,$$

with ΔH_n for

$$(CH_3OH)_n \rightarrow (CH_3OH)_{n-1}H^+ + CH_3O$$

calculated based on the same thermodynamic cycle employed for water clusters (see Figs. 7 and 8). The $\Delta_a H_{n-1,n}$ is the reaction energy of a protonated methanol cluster ion $(CH_3OH)_{n-1}H^+$ combining with a methanol molecule. $\Delta_b H_{n,n+1}$ is the reaction energy of the neutral cluster $(CH_3OH)_n$ combining with a methanol molecule, and can be generated from theoretical calculations.[57] The appearance energy of the $CH_3OH_2^+$ product has been measured as 10.5 eV as follows:[21]

$$(CH_3OH)_2 \rightarrow (CH_3OH)H^+ + CH_3O, \quad \Delta H_2 = 10.5\ \mathrm{eV}. \tag{12}$$

Thus $\Delta H_3, \Delta H_4, \ldots, \Delta H_{10}$ can be calculated and are listed in Table II. ΔH_n is the minimum energy required for the initiation of reaction (12) without excess energy used for the metastable dissociation of protonated methanol cluster ions.

The VIE for larger methanol clusters is not known, but it should not change much with increasing cluster size. Based on a study by Cook *et al.*,[58] the VIE of $(CH_3OH)_5$ is about 9.9 eV; the VIE for $5 \leqslant n \leqslant 10$ is thereby taken as 9.9 eV. The calculated results for E_{excess} for these clusters are given in Table II. Comparing the cluster ion dissociation energies $E_{dissoc,n}$ to their excess energies $E_{excess,n}$, thus obtained, one finds that $E_{excess,n} < E_{dissoc,n}$. In other words, the energy deposited in the cluster upon ionization is not enough to dissociate the metastable clusters as rapidly as is observed experimentally. The extra (thermal) energy must come from the neutral cluster, and the difference between E_{dissoc} and E_{excess} must be E_{therm}. $E_{therm,n}$ then generates a temperature for each neutral cluster in the supersonic beam.

Neutral cluster temperatures are presented in Table II. These vary from 50 to 100 K for neutral clusters $6 \leqslant n \leqslant 11$. These temperatures appear reasonable when compared with those obtained for neutral water clusters (Table I). The temperatures of neutral water are about 40–100 K for the sizes $n=10-15$. According to theoretical calculations, the binding energies of neutral water clusters and methanol clusters are similar (ca. 1800–2000 cm^{-1} for the dimers). Since the exact VIE is not known experimentally for methanol clusters, the temperatures reported here should be thought of as an estimate of the internal energy of the neutral clusters.

C. Ammonia clusters

1. Distribution of ammonia clusters ionized by a soft x-ray laser

Figure 12 presents a typical reflection TOFMS of ammonia clusters ionized at 26.5 eV by single photon ionization. Most of the prominent features in the spectrum are identified as protonated ammonia cluster ions with the general formula $(NH_3)_nH^+$. They are generated, as by now expected, from intracluster ion-molecule reactions upon ionization of the neutral clusters in the molecular beam. For single photon ionization this reaction has been proposed as an absorption-ionization-dissociation mechanism,

$$(NH_3)_n + h\nu \rightarrow [(NH_3)_n^+]^* + e^- \rightarrow (NH_3)_{n-1}H^+ + NH_2 + e^-. \tag{13}$$

Intensities of protonated ammonia cluster ions decrease roughly exponentially with increasing cluster size n. A significant drop in intensity occurs at $n=6$ and special cluster ion sizes are not observed in the spectrum. A similar behavior for this system has been observed by other ionization techniques such as EI,[30,31] nanosecond laser MPI,[32,33] femto-

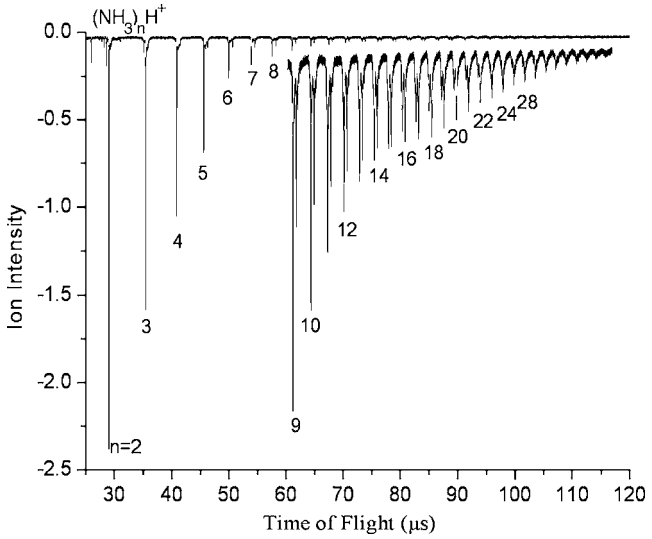

FIG. 12. A reflectron TOF mass spectrum of ammonia clusters ionized by a 26.5 eV soft x-ray laser.

second laser MPI,[34,35] and single photon ionization.[36] A high resolution spectrum for small clusters is presented in Fig. 13. Five different series of cluster ions are identified in this mass range. These are labeled A_n, B_n, P_n, D_n, E_n in Fig. 13. The peaks labeled P_n represent parent ions of the protonated ammonia cluster series. P_n are generated from the neutral clusters $(NH_3)_{n+1}$ by intracluster ion-molecule reaction upon ionization. They dominate the spectrum at small cluster sizes up to $n=14$. Peaks marked D_n are daughter ions of the parent protonated ammonia clusters. They are created by the unimolecular dissociation of P_{n+1}, $(NH_3)_{n+1}H^+ \rightarrow (NH_3)_nH^+ + NH_3$, in the first field-free region of the reflectron TOFMS. In the absence of collision induced dissociation processes, only one ammonia molecule is lost for each parent protonated cluster ion for all observed clusters $5 \leqslant n \leqslant 22$. Daughter ion signals dominate the spectrum for larger ammonia clusters, $n \geqslant 14$.

The cluster ion series labeled B_n can also be observed in the mass spectrum presented in Fig. 13: these species can be identified for $5 \leqslant n \leqslant 12$ in our experiments. This series of clusters is observed for $n \sim 25$ by EI ionization.[59] These clusters have been suggested to have the formula $(NH_3)_nH_2^+$. Series B_n features can be generated from an intracluster ion-molecule reaction as follows:

$$(NH_3)_{n+1}^+ \rightarrow (NH_3)_nH_2^+ + NH. \tag{14}$$

Some part of the intensity of these features could arise from the presence of water in the clusters as $(NH_3)_{n-2}(H_2O)NH_4^+$ and $(NH_3)_{n-1}H_2^+$ have the same mass.

Another series of cluster ions labeled E_n is identified as $(NH_3)_{n-1}NH_2^+$ in Fig. 13. This series is generated from the neutral cluster $(NH_3)_n$ by the loss of one H atom during the ionization process,

$$(NH_3)_n + h\nu \rightarrow [(NH_3)_n^+]^* + e^- \rightarrow (NH_3)_{n-1}NH_2^+ + H + e^-. \tag{15}$$

The remaining (fifth) series as shown in Fig. 13 is discussed in the next section and is labeled A_n $[(NH_3)_n^+]$.

2. Unprotonated ammonia cluster ions $(NH_3)_n^+$

Figure 13 also shows unprotonated ammonia cluster ions labeled A_n (observed for $2 \leqslant n \leqslant 20$). They are formed by direct ionization of $(NH_3)_n$ neutral clusters that do not undergo a proton transfer reaction or a fragmentation reaction following ionization with a single photon of 26.5 eV. A plot of the unprotonated cluster ion intensity as a function of cluster size n is presented in Fig. 14. The intensity distribution of $(NH_3)_n^+$ exhibits a sharp decrease at $n=6$, increases slowly to $n=10$, and then decreases again with increasing n. Also plotted in Fig. 14 is the intensity ratio $(NH_3)_n^+/(NH_3)_{n-1}H^+$, both components of which come from the same neutral parent clusters $(NH_3)_n$. This ratio has a distinct minimum at $n=6$ and a maximum at $n=15$. These patterns imply that proton transfer reactions proceed more

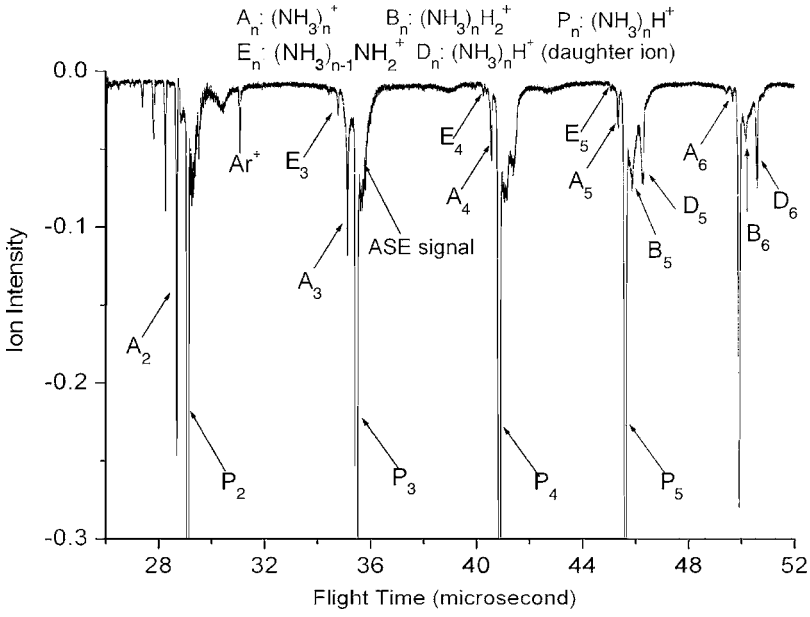

FIG. 13. A high-resolution reflectron TOF mass spectrum of small ammonia clusters ionized by a 26.5 eV soft x-ray laser. A_n: unprotonated cluster ions generated directly from the ionization of neutral ammonia clusters $(NH_3)_n$. P_n: parent protonated ammonia ions generated from a neutral cluster $(NH_3)_{n+1}$. D_n: daughter ions formed from parent ions P_{n+1} via loss of one NH_3 molecule. B_n: one mass larger than protonated ammonia ions. They are generated from $(NH_3)_{n+1}$ via losing NH after ionization. E_n: one mass smaller than $(NH_3)^+$ ions. they are generated from $(NH_3)_n$ via loss of one H atom during the ionization process.

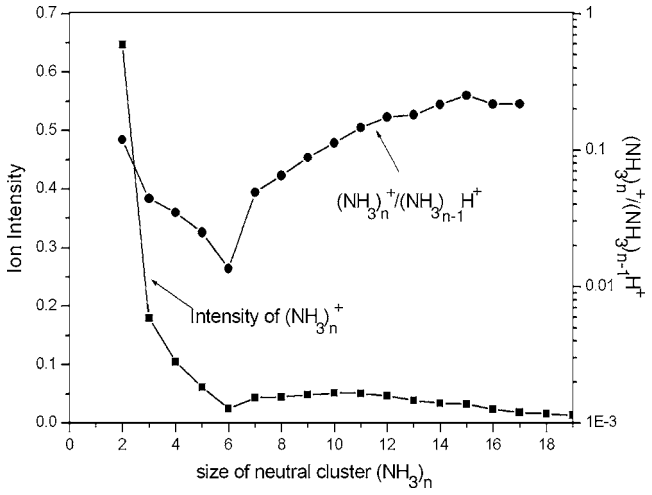

FIG. 14. Plots of the intensity distributions of unprotonated ammonia clusters and intensity ratio distributions of $(NH_3)_n/(NH_3)_{n-1}H^+$ as a function of cluster size n.

rapidly for $n=6$, which in turn seems to suggest an enhanced structured stability for $(NH_3)_5H^+$. Note the reduction in relative intensity for $(NH_3)_6H^+$ in Fig. 12.

A comparison of these results with those generated with atomic resonance lamp radiation [Ar (11.83 and 11.62 eV), Kr (10.64 and 10.03 eV), and Xe (9.57 eV)] employed for ionization[36] proves interesting. In both experiments a single photon is absorbed by a neutral ammonia cluster for ionization, but the photon energies are quite different; nonetheless, similar trends are observed in the distribution of unprotonated ammonia clusters in all instances. For resonance lamp ionization, unprotonated ammonia cluster ions are observed for $n=2-25$, and the intensity ratios $(NH_3)_n^+/(NH_3)_{n-1}H^+$ have a minimum at $n=6$. The largest intensity for the $(NH_3)_2^+$ is observed with Xe (9.57 eV) ionization and the $(NH_3)_2^+$ intensity decreases for Kr and Ar lamp ionizations. This behavior is not observed for $(NH_3)_n^+$ with $n \geqslant 3$. The 26.5 eV ionization intensities resemble those for Kr lamp ionization. EI ionization finds $(NH_3)_n^+$ features only for $n \geqslant 10$ and these signals depend on the electron energy.[36] Again these comparisons relate the usefulness of single photon ionization and demonstrate the fact that the ionized electron carries with it most, if not all, of the excess photon energy above the VIE of the neutral cluster.

3. Photolysis of NH_3, $(NH_3)_2$, and $(NH_3)_3$

As shown in Fig. 15(a), product species NH_3^+, NH_2^+, and NH^+ are observed from the ionization of NH_3 by a 26.5 eV photon. The main product from this ionization is NH_2^+. The appearance energy for NH_2^+ from NH_3 is 15.8 eV.[60] Intensity of the NH_2^+ ion feature is about 1.7 times larger than that of the NH_3^+ ion. Only a small intensity is detected for the NH^+ ion, whose threshold is 17.1 eV.[61] Three channels are identified for the photolysis/ionization of NH_3 by a 26.5 eV photon as follows:

$$NH_3 + h\nu(26.5\ \text{eV}) \rightarrow NH_3^+ + e^- \quad 36\% \tag{16a}$$

$$\rightarrow NH_2^+ + H + e^- \quad 62.6\% \tag{16b}$$

$$\rightarrow NH^+ + 2H + e^- \quad 1.3\%\ . \tag{16c}$$

The percentage values in Eq. (1b) are the branching ratio for these reactions.

The $(NH_3)_2$ photolysis/ionization products are shown in Figs. 15(b) and 15(a) (NH_4^+). Product channels can be identified as follows:

$$(NH_3)_2 + h\nu(26.5\ \text{eV}) \rightarrow NH_4^+ + NH_2 + e^- \quad 84\% \tag{17a}$$

$$\rightarrow (NH_3)_2^+ + e^- \quad 9.9\% \tag{17b}$$

$$\rightarrow NH_3NH_2^+ + H + e^- \quad 3.6\% \tag{17c}$$

$$\rightarrow (NH_3)NH^+/(NH_2)_2^+ + 2H + e^- \quad \leqslant 1.7\% \tag{17d}$$

$$\rightarrow NH_2NH^+ + 3H + e^- \quad < 1\% \tag{17e}$$

$$\rightarrow NHNH^+ + 4H + e^- \quad < 1\% \tag{17f}$$

$$\rightarrow NNH^+ + 5H + e^- \quad < 1\%\ . \tag{17g}$$

The main product (NH_4^+) from the dimer photoionization is generated by an intracluster ion-molecular reaction as found for the other clusters discussed in this report. The product $(NH_2)_2^+$ is observed in an argon expansion ionized by an ArF excimer at 193 nm (6.42 eV).[67] Mass features at 28 and 32 amu could also have contamination by N_2 and O_2, respectively, which exist in the background gas ($\sim 10^{-6}$ Torr) in the vacuum chamber, and perhaps in the expansion He gas as well. The fact that $(NH_3)_2$ displays different ionization properties than water and methanol dimers may be related to its different cluster structure and (dipole-dipole) bonding arrangement.[1,2] The weaker intermolecular interactions for

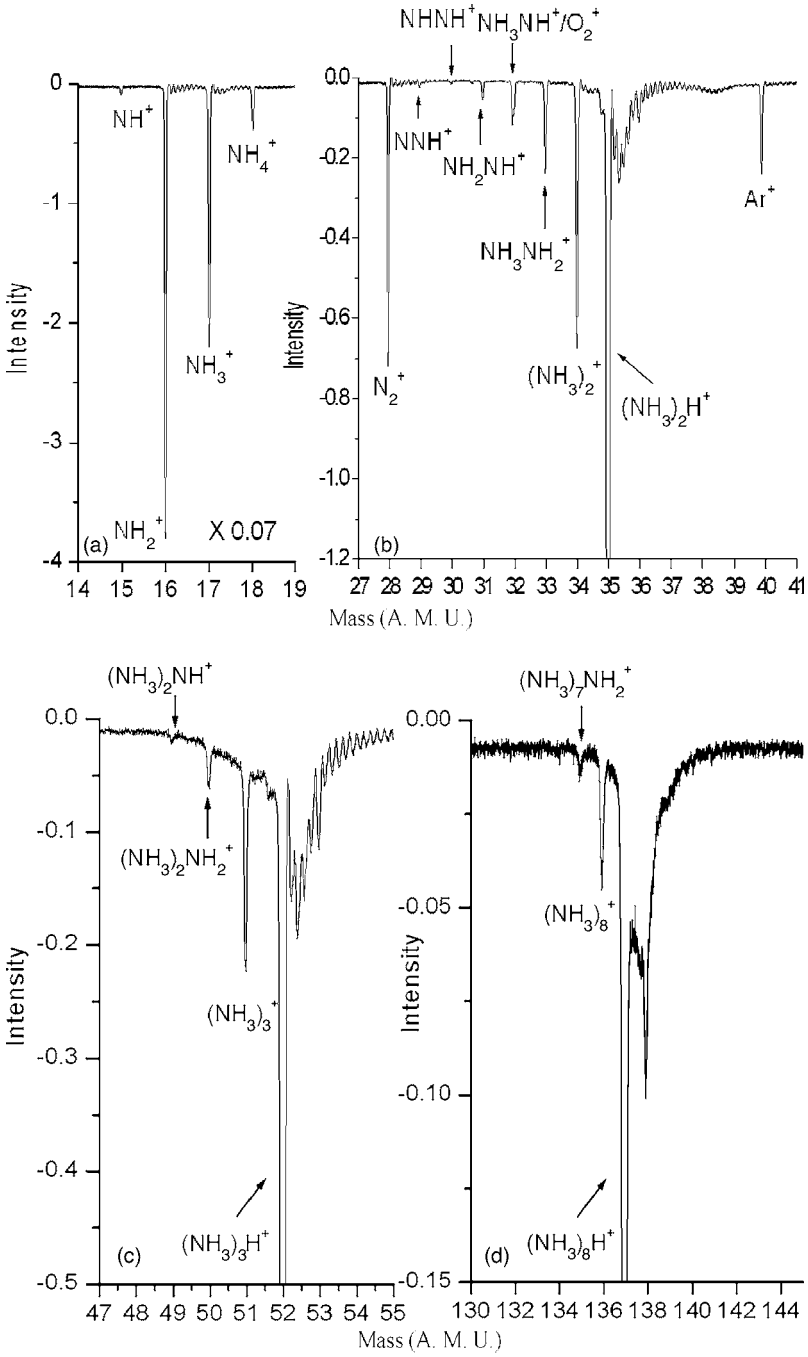

FIG. 15. Mass spectra of (A) NH_3, (B) $(NH_3)_2$, (C) $(NH_3)_3$, and (D) $(NH_3)_8$ ionized by a 26.5 eV soft x-ray laser, respectively.

$(NH_3)_2$ vs $(H_2O)_2$ and $(CH_3OH)_2$ may also account for its different products that can arise by a greater localization of the absorbed photon energy.

Products $(NH_3)_2H^+$ (P_2), $(NH_3)_3^+$, $(NH_3)_2^+$, and $(NH_3)_2NH^+$ are observed from photodissociation/ionization of the neutral ammonia trimer $(NH_3)_3$ as shown in Figs. 15(b) and 15(c). They are generated in the following reaction channels:

$$(NH_3)_3 + h\nu(26.5\ \text{eV}) \rightarrow (NH_3)_2H^+ + NH_2 + e^- \quad 94.8\% \tag{18a}$$

$$\rightarrow (NH_3)_3^+ + e^- \quad 4.2\% \tag{18b}$$

$$\rightarrow (NH_3)_2NH_2^+ + H + e^- \quad < 1.0\% \tag{18c}$$

$$\rightarrow (NH_3)_2NH^+ + 2H + e^- \quad < 0.2\%\ . \tag{18d}$$

The $(NH_3)_2H^+$ ion [Fig. 15(b)] is the main product as usual, and $(NH_3)_3^+$ is generated by direct ionization of the trimer without the subsequent proton transfer reaction.

The mechanism of photolysis/ionization of neutral $(NH_3)_3$ is apparently different from that of the dimer. Products with the loss of more than three H atoms are not observed in the spectrum of the neutral trimer, but are observed in the dimer spectrum. As shown in Fig. 15(d), only the loss

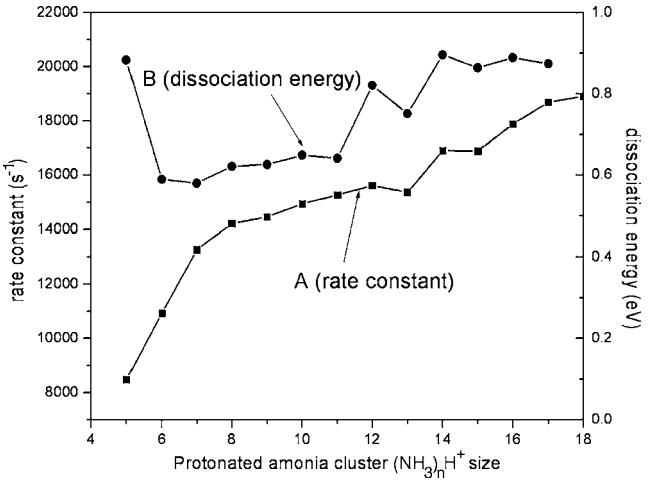

FIG. 16. Metastable dissociation rate constants (A) and dissociation energies (B) for protonated ammonia clusters generated from the experimental data for 26.5 eV ionization.

of one H atom is observed for larger clusters. Clusters of the form $(NH_3)_nNH_2^+$ are also observed by EI ionization[59] and MPI;[62] these latter species are not observed, however, with vuv resonance lamp ionization[36] for which only $(NH_3)_nH^+$ and $(NH_3)_n^+$ cluster ions are detected. This implies that the loss of one H atom to generate $(NH_3)_{n-1}NH_2^+$ cluster ions requires more energy than the proton transfer reaction to generate $(NH_3)_{n-1}H^+$, and that the proton transfer reaction is more favorable for larger clusters. The larger $(NH_3)_n$ clusters have a greater proton affinity than do smaller ones.[49,63]

As noted above, the structure of $(NH_3)_n$, $(CH_3OH)_n$, and $(H_2O)_n$ are very different due to the dominance of dipole-dipole interactions for $(NH_3)_n$ and hydrogen bonding interactions for $(CH_3OH)_n$ and $(H_2O)_n$ clusters. Such structural and potential differences may also be related to the difference in small cluster ($n=2,3$) chemistry for these species. The photon energy absorbed by the cluster following ionization may remain localized longer in the weakly bonded ($\sim$1000 cm^{-1}/dimer) ammonia system than in the more strongly bonded ($\sim$1800–2200 cm^{-1}/dimer) water and methanol systems, and thus may be responsible for the more varied "molecular" chemistry found for the ammonia cluster system.

4. Dissociation rate constants of metastable ammonia cluster ions

The unimolecular dissociation rate constant of protonated ammonia cluster ions can be obtained from the decay fraction of the parent ion in much the same way as described above for $(H_2O)_nH^+$ and $(CH_3OH)_nH^+$ clusters. As shown in Fig. 16, the rate constant for the unimolecular reaction $(NH_3)_nH^+ \rightarrow (NH_3)_{n-1}H^+ + NH_3$ is about $(0.8-2)\times 10^4$ s^{-1} and increases with increasing n in the cluster ion range $5 \leqslant n \leqslant 18$. In the experiment of Wei *et al.*,[64] unimolecular dissociation rate constants are observed for this cluster series and a value of $k_{17}=1.7\times 10^4$ s^{-1} is found: our values for k_{17} is 1.9×10^4 s^{-1}.

If a rate constant is obtained for a unimolecular reaction, a value for E_{dissoc} can be obtained based on classical RRK calculations [see Eq. (4)]. Values of E_{bind} are taken from Ref. 49 and k_n are taken from our experimental data. Ammonia has two low energy vibrational modes (932 and 968 cm^{-1}). For large clusters these modes can contribute to the cluster vibrational degrees of freedom required for statistical ergodic calculations of rate constants: we thus, following the lead for water clusters, use $S=6.6n-6$. Values of E_{dissoc} for the metastable dissociation of the loss of one NH_3 molecule from $(NH_3)_nH^+$ ($P_n \rightarrow D_{n-1}$) in the first field-free region of the reflectron TOFMS are shown in Fig. 16 and listed in Table III. Note that at $n=5$, much more energy is required for the dissociation of $(NH_3)_5H^+$ than for the other cluster ions; the reason for this increased dissociation energy $E_{\text{dissoc},5}$ is that the binding energy for this cluster ion $E_{\text{bind},5}$ is much larger than $E_{\text{bind},n}$ and other larger clusters (see Table III) for n up to $\sim$15.

TABLE III. Data used to calculate the vibrational temperature of neutral ammonia clusters in the molecule beam.

n	E_{dissoc} (eV)[a] $(NH_3)H^+$	$\Delta_aH_{n-1,n}$ (eV)[b]	$\Delta_bH_{n,n-1}$ (eV)[c]	ΔH_n (eV)[d] $(NH_3)_n$
5	0.954	0.527	0.260	8.661
6	0.640	0.3	0.240	8.394
7	0.632	0.257	0.256	8.334
8	0.678	0.243	0.232	8.334
9	0.683	0.22	0.265	8.323
10	0.709	0.2077	0.245	8.368
11	0.701	0.187	0.312	8.406
12	0.898	0.22	0.198	8.532
13	0.822	0.187	0.265	8.510
14	0.981	0.207	0.254	8.588
15	0.947	0.187	0.286	8.635
16	0.9742	0.18	0.259	8.736
17	0.9586	0.168	0.273	8.813

[a]Calculated based on dissociation rate constant obtained in the present experiment.
[b]Taken from experimental data of Ref. 49.
[c]Taken from theoretical calculations of Ref. 63.
[d]Calculated based on the same thermodynamic cycles employed for the water cluster in Fig. 8.

5. Ammonia cluster temperature

In the present experiments, the ammonia cluster ion distribution is observed in the mass spectrum and even unprotonated cluster ions ($2 \leqslant n \leqslant 20$) can be observed (see Figs. 12–14). One can assume that the energy above the VIE is removed by the ejected electron, as done previously for $(H_2O)_n$ and $(CH_3OH)_n$ clusters. Neglecting translational energy release for the products, the residual energy (E_{excess}) needed to dissociate the $(NH_3)_nH^+$ cluster ions can be calculated: $E_{\text{excess}}=\text{VIE}-\Delta H_n$ according to Eq. (6), and $\Delta H_{n+1}=\Delta H_n+\Delta_aH_{n-1,n}-\Delta_bH_{n,n+1}$. Thus ΔH_n for ammonia cluster ions can be calculated as has been done above for the water and methanol species. Here, $\Delta_aH_{n-1,n}$ is the reaction energy for the protonated cluster ion $(NH_3)_{n-1}H^+$ and an ammonia monomer,[49] and $\Delta_bH_{n,n+1}$ is the reaction energy for neutral

$(NH_3)_n$ and an ammonia monomer.[63] Ceyer *et al.*[28] have measured ΔH_3 for $(NH_3)_3H^+$ generation from $(NH_3)_4$ as follows:

$$(NH_3)_4 \rightarrow (NH_3)_3H^+ + NH_2 + e^-, \quad \Delta H_4 = 9.03 \text{ eV}, \tag{19}$$

and thereby $\Delta H_5, \Delta H_6, \ldots, \Delta H_n$ can be calculated. This ΔH_n value represents the minimum energy required for the reaction $(NH_3)_n \rightarrow (NH_3)_{n-1}H^+ + NH_2$ to occur, without excess energy remaining in the cluster ion for metastable dissociation of the protonated ammonia cluster to occur in the first field-free region of the TOFMS drift tube. Values of ΔH_n for ammonia clusters $(10 \leqslant n \leqslant 21)$ are listed in Table III. Unlike the situation found for water and methanol cluster ions (Tables I and II), ΔH_n for ammonia cluster ions increases with increasing n, since $\Delta_a H_{n-1,n}$ is smaller than $\Delta_b H_{n,n+1}$. But this trend is different than that observed for water and methanol cluster ions: for these other clusters, ΔH_n decreases with increasing n and then tends to a constant value for large cluster sizes (see Tables I and II). For ammonia clusters, the cluster binding energy $(\Delta_a H_{n-1,n})$ of protonated cluster ions and the cluster binding energy $(\Delta_b H_{n,n+1})$ of neutral clusters do not match well for the calculation of ΔH_n. So the thermal properties and temperature of neutral ammonia clusters cannot be estimated as is done above for water and methanol clusters, even though the qualitative interaction and data set appear the same for all these species. This difficulty could be due to a real difference for $(NH_3)_n$ vs $(H_2O)_n$ and $(CH_3OH)_n$ or it could be due to an inconsistency in the required thermodynamic $(NH_3)_n$ data set for this procedure. While at this time we cannot be certain which of these possibilities is correct, we favor the second explanation for the inability to generate a consistent and small set of temperatures for the ammonia cluster system.

If we accept that the cause of our inability to assign a set of temperatures to ammonia clusters has to do with an inconsistent data set for these species, the three cluster systems present an impressively similar set of quantitative properties and behaviors with regard to species and trends (see Figs. 6, 11, and 16). Note too that the three systems have considerably different structures, bonding patterns, and bonding energies. In other words statistical, ergodic, RRK/RRKM dynamics hold for all cases and the structural details and different limiting potentials for these three systems play a relatively minor role in their chemistry.

IV. SUMMARY AND CONCLUSIONS

The very compact 26.5 eV soft x-ray laser is a near ideal ionization source with which to investigate weakly bound (hydrogen bonded and van der Waals) clusters in the gas phase. In this work, water, methanol, and ammonia clusters are ionized by a single 26.5 eV laser photon. The advantage of single photon ionization is that it prevents or hinders cluster fragmentation after ionization. This is typically not the case for nanosecond multiphoton ionization. Although 26.5 eV energy is initially absorbed by the neutral cluster, almost all the energy above the VIE is removed by the ejected photoelectron. Metastable dissociation of cluster ions can thereby be understood and characterized through the internal intracluster reaction energies and neutral cluster temperature.

Protonated water clusters up to $n=60$ are observed in mass spectra. The intensity of these cluster ions decreases roughly exponentially with increasing cluster size. The parent water cluster ion does not show any special signal ("magic number") intensity at $(H_2O)_{21}H^+$, and the enhanced intensity at $n=21$ is due to the fast dissociation of $(H_2O)_{22}H^+$ in the drift tube. A small signal of unprotonated water dimer ion is observed if pure He is used as the carrier gas for the supersonic expansion. This unprotonated dimer signal intensity increases if the concentration of Ar in the carrier gas is increased, due to the formation of binary clusters $Ar_m(H_2O)_n$. These mixed clusters undergo rapid dissociation of Ar_m during the ionization/fragmentation process and this dissociation removes enough energy from the cluster to impede the proton transfer/fragmentation reaction. The unimolecular dissociation rate constant for protonated water cluster ions is $(0.6-2.7)\times 10^4$ s^{-1} for clusters of $8 \leqslant n \leqslant 24$. The vibrational temperatures of neutral water clusters are in the range of 40–200 K for the clusters $10 \leqslant n \leqslant 21$, based on the rate constants, excess energies, and calculated thermodynamics for $(H_2O)_n$.

The major series of protonated methanol clusters is observed in the mass spectrum with no abnormal or magic number signals. The cluster ion signal intensity decreases roughly exponentially with increasing cluster size. The only unprotonated methanol cluster observed is the dimer. Cluster ions of the form $(CH_3OH)_nH_3O^+$, generated from an intracluster ion-molecule reaction and loss of $(CH_3)_2O$, are not observed in the mass spectrum because only a small amount of excess energy is deposited in neutral clusters employing single photon 26.5 eV ionization. Products CH_3^+, CHO^+, CH_2O^+, CH_2OH^+ and CH_3OH^+ are observed in the photolysis/ionization of the CH_3OH monomer. At this energy, rate constants for the metastable dissociation of protonated methanol cluster ions are obtained in the range of $(3.6-6.0)\times 10^{+3}$ s^{-1} for cluster sizes $5 \leqslant n \leqslant 10$. Vibrational temperatures of neutral methanol clusters are about 50–100 K for the cluster range $6 \leqslant n \leqslant 10$.

Protonated ammonia cluster ions dominate the ammonia cluster mass spectrum, as usual for the other two systems discussed, and signal intensity decreases roughly exponentially with increasing cluster size. Unprotonated clusters are observed in the range $2 \leqslant n \leqslant 22$. The intensity distribution for unprotonated cluster ions exhibits a distinct minimum at $n=6$. This intensity decrease implies a more rapid proton transfer reaction process for the $(NH_3)_6^+$ cluster and enhanced structural stability of the $(NH_3)_5H^+$ cluster ion. Products for the loss of up to five H atoms in the photolysis/ionization process for the neutral ammonia dimer are observed. Loss of more than three H atoms is not observed in the mass spectrum of larger $(n \geqslant 3)$ cluster ions. The unimolecular metastable dissociation rate constants for protonated ammonia cluster ions are found to be between (0.8 and 2.0) $\times 10^4$ s^{-1} for $5 \leqslant n \leqslant 18$. A cluster temperature range for $(NH_3)_n$ neutral clusters could not at present be characterized [as accom-

plished for (H_2O) and $(CH_3OH)_n$] most probably due to inconsistencies within the existing thermodynamic data set for this system.

ACKNOWLEDGMENT

This work was supported by the NSF ERC for Extreme Ultraviolet Science and Technology under NSF Award No. EEC-0310717.

[1] D. D. Nelson, Jr., G. T. Fraser, and W. Klemperer, Science **238**, 1670 (1987).
[2] W. Klemperer, Science **257**, 887 (1992).
[3] R. G. Keesee, J. Geophys. Res. **94**, 14683 (1989).
[4] G. Nidener-Shatteburg and V. E. Bondybey, Chem. Rev. (Washington, D.C.) **100**, 4059 (2000).
[5] W. W. Duley, Astrophys. J. Lett. **471**, L57 (1996).
[6] A. Hansel, W. Singer, A. Wisthaler, M. Schwarzmann, and W. Lindinger, Int. J. Mass Spectrom. Ion Process. **167/168**, 697 (1997).
[7] O. Echt, D. Kreisle, M. Knapp, and E. Recknagel, Chem. Phys. Lett. **108**, 401 (1984).
[8] U. Nagashima, H. Shinohara, N. Nishi, and H. Tanaka, J. Chem. Phys. **84**, 209 (1986).
[9] M. Okumura, L. I. Yeh, J. D. Myers, and Y. T. Lee, J. Phys. Chem. **94**, 3416 (1990).
[10] L. I. Yeh, M. Okumura, J. D. Myers, J. M. Price, and Y. T. Lee, J. Chem. Phys. **91**, 7319 (1989).
[11] Z. Shi, J. V. Ford, S. Wei, and A. W. Castleman, Jr., J. Chem. Phys. **99**, 8009 (1993).
[12] H. Shiromaru, N. Nishi, and N. Washida, J. Chem. Phys. **84**, 5561 (1986).
[13] P. P. Radi, P. Beaud, D. Franzke, H.-M. Frey, T. Gerber, B. Mischler, and A.-P. Tzannis, J. Chem. Phys. **111**, 512 (1999).
[14] V. Hermann, B. D. Kay, and A. W. Castleman, Jr., Chem. Phys. **72**, 185 (1982).
[15] X. Yang, X. Zhang, and A. W. Castleman, Jr., Int. J. Mass Spectrom. Ion Process. **109**, 339 (1991).
[16] S. Wei, Z. Shi, and A. W. Castleman, Jr., J. Chem. Phys. **94**, 3268 (1991).
[17] J. Stace and C. Moore, Chem. Phys. Lett. **96**, 80 (1983).
[18] S. K. Chowdhury and B. T. Chait, Anal. Chem. **63**, 1660 (1991).
[19] T. Schindler, C. Berg, G. Niedner-Schatteburg, and V. E. Bondybey, Chem. Phys. Lett. **250**, 301 (1996).
[20] H. Chang, C. Wu, and J. Kuo, Int. Rev. Phys. Chem. **24**, 553 (2005).
[21] G. Vaidyanathan, M. T. Coolbaugh, W. R. Peifer, and J. F. Garvey, J. Chem. Phys. **94**, 1850 (1991).
[22] M. S. EI-Shall, C. Marks, L. W. Sieck, and M. Meot-Ner, J. Phys. Chem. **96**, 2045 (1992).
[23] S. Morgan, R. G. Keesee, and A. W. Castleman, Jr., J. Am. Chem. Soc. **111**, 3841 (1989).
[24] S. Morgan and A. W. Castleman, Jr., J. Am. Chem. Soc. **109**, 2867 (1987).
[25] S. Morgan and A. W. Castleman, Jr., J. Phys. Chem. **93**, 4544 (1989).
[26] H. Fu, Y. J. Hu, and E. R. Bernstein, J. Chem. Phys. **124**, 024302 (2006).
[27] Y. J. Shi, S. Consta, A. K. Das, B. Mallik, D. Lacey, and R. H. Lipson, J. Chem. Phys. **116**, 6990 (2002).
[28] S. T. Ceyer, P. W. Tiedemann, B. H. Mahan, and Y. T. Lee, J. Chem. Phys. **70**, 14 (1979).
[29] C. Y. Ng, D. J. Trevor, P. W. Tiedemann, S. T. Ceyer, P. L. Kronebusch, B. H. Mahan, and Y. T. Lee, J. Chem. Phys. **67**, 4235 (1977).
[30] J. A. Odutola, T. R. Dyke, B. J. Howard, and J. S. Muenter, J. Chem. Phys. **70**, 4884 (1979).
[31] K. Stephan, J. H. Futrell, K. I. Peterson, A. N. Castleman, Jr., H. E. Wagner, N. Djuric, and T. D. Mark, Int. J. Mass Spectrom. Ion Phys. **44**, 167 (1982).
[32] S. Wei and A. W. Castleman, Jr., Int. J. Mass Spectrom. Ion Process. **131**, 133 (1994).
[33] H. Shinohara and N. Nishi, Chem. Phys. Lett. **87**, 561 (1982).
[34] D. A. Card, D. E. Folmer, S. A. Buzza, and A. W. Castleman, Jr., J. Phys. Chem. A **101**, 3417 (1997).
[35] S. A. Buzza, S. Wei, J. Purnell, and A. W. Castleman, Jr., J. Chem. Phys. **102**, 4832 (1995).
[36] H. Shinohara and N. Nishi, J. Chem. Phys. **83**, 1939 (1985).
[37] D. N. Shin, Y. Matsuda, and E. R. Bernstein, J. Chem. Phys. **120**, 4150 (2004).
[38] Y. Matsuda and E. R. Bernstein, J. Phys. Chem. A **109**, 3803 (2005).
[39] S. Tomoda and K. Kimura, Chem. Phys. Lett. **102**, 560 (1983).
[40] (a) S. Heinbuch, M. Grisham, D. Martz, and J. J. Rocca, Opt. Express **13**, 4050 (2005); (b) J. J. Rocca, V. N. Shlyaptsev, F. G. Tomasel, O. D. Cortazar, D. Hartshorn, and J. L. A. Chilla, Phys. Rev. Lett. **73**, 2192 (1994); (c) J. J. Rocca, Rev. Sci. Instrum. **70**, 3799 (1999).
[41] Yu. A. Uspenskii, V. E. Levashov, A. Vinogradov, A. I. Fedorenko, V. V. Kondratenko, Yu. P. Pershin, E. N. Zubarev, and V. Yu. Fedotov, Opt. Lett. **23**, 771 (1998).
[42] M. W. Jurema, K. N. Kirschner, and G. C. Shields, J. Comput. Chem. **14**, 1326 (1993).
[43] K. Laasonen and M. L. Klein, J. Phys. Chem. **98**, 10079 (1994).
[44] M. Svanberg and J. B. C. Pettersson, J. Phys. Chem. A **102**, 1865 (1998).
[45] I. Kusaka and D. W. Oxtoby, J. Chem. Phys. **113**, 10100 (2000).
[46] M. P. Hodges and D. J. Wales, Chem. Phys. Lett. **324**, 279 (2000).
[47] H. Shiromaru, H. Shinohara, N. Washida, H. S. Yoo, and K. Kimura, Chem. Phys. Lett. **141**, 7 (1987).
[48] O. Echt, P. P. S. Morgan, and A. W. Castleman, Jr., J. Chem. Phys. **82**, 4076 (1985).
[49] S. Wei, W. B. Tzeng, and A. W. Castleman, Jr., J. Chem. Phys. **93**, 2506 (1990).
[50] W. B. Tzeng, S. Wei, and A. W. Castleman, Jr., J. Am. Chem. Soc. **111**, 6035 (1985).
[51] P. J. Robinson and K. A. Holbrook, *Unimolecular Reaction* (Wiley Interscience, New York, 1971), p. 53.
[52] S. Wei, K. Kilgore, W. B. Tzeng, and A. W. Castleman, Jr., J. Phys. Chem. **95**, 8306 (1991).
[53] J. T. Su, X. Xu, and W. A. Goddard III, J. Phys. Chem. A **108**, 10518 (2004).
[54] I. P. Buffey and W. B. Brown, Chem. Phys. Lett. **109**, 59 (1984).
[55] T. D. Fridgen, J. D. Keller, and T. B. McMahon, J. Phys. Chem. A **105**, 3816 (2001).
[56] E. P. Grimsrud and P. Kebarle, J. Am. Chem. Soc. **95**, 7939 (1973).
[57] U. Buck, J. G. Siebers, and R. J. Wheatley, J. Chem. Phys. **108**, 20 (1998).
[58] K. D. Cook, G. G. Jones, and J. W. Taylor, Int. J. Mass Spectrom. Ion Phys. **35**, 273 (1980).
[59] W. R. Peifer, M. T. Coolbaugh, and J. F. Garvey, J. Chem. Phys. **91**, 6684 (1989).
[60] J. E. McCulloh, Int. J. Mass Spectrom. Ion Phys. **21**, 33 (1976).
[61] R. I. Reed and W. Snedden, J. Chem. Soc. **1959**, 4132.
[62] M. Farber and F. Huisken, J. Chem. Phys. **104**, 4865 (1996).
[63] T. A. Beu and U. Buck, J. Chem. Phys. **114**, 7848 (2001).
[64] S. Wei, W. B. Tzeng, and A. W. Castleman, Jr., J. Chem. Phys. **92**, 332 (1990).
[65] H. Shinohara, N. Nishi, and N. Washida, J. Chem. Phys. **83**, 1939 (1985).
[66] T. Shimanouchi, *Tables of Molecular Vibrational Frequencies*, Natl. Bur. Stand. (U.S.) Circ. No. 39 (U.S. GPO, Washington, D.C., 1972), Vol. I, pp. 1–160.
[67] M. Farber and F. Huisken, J. Chem. Phys. **104**, 4865 (1996).